PhD degree in Systems Medicine (curriculum in Molecular Oncology)

European School of Molecular Medicine (SEMM),

University of Milan and University of Naples "Federico II"

Settore disciplinare: Med/04

Interferon Regulatory Factor 1 (IRF1) links immunological and metabolic traits to histological grade in pancreatic cancer

Gabriele Alfarano

IEO, Milan

Matricola n. R11148-R20

Supervisor: Myriam Alcalay

IEO, Milan

Added Supervisor:

Gioacchino Natoli

IEO, Milan

Humanitas University, Rozzano (MI)

Anno accademico 2017-2018

Table of contents

I. Index of the figures

II. List of abbreviations

PDAC	Pancreatic Ductal Adenocarcinoma
TF(s)	Transcription Factor(s)
G1/G2/G3	Grade 1/2/3
IRF1	Interferon Regulatory Factor 1
IFN(α/β/γ)	Interferon (alpha/beta/gamma)
ISG(s)	Interferon Stimulated Gene(s)
ADM	Acinar-to-Ductal Metaplasia
IPMN	Intra Papillary Mucinous Neoplasm
MCN	Mucinous Cystic Neoplasm
EMT	Epithelial-to-Mesenchymal Transition
WT	Wild Type
KO	Knock Out
H&E	Haematoxylin and Eosin
DEG	Differentially Expressed Gene
FDR	False Discovery Rate
GO	Gene Ontology
GSEA	Gene Set Enrichment Analysis
MHC/HLA	Major Histocompatibility Complex/Human Leukocyte Antigen
TCA cycle	TriCarboxylic Acid cycle
LC-ESI	Liquid Chromatography-ElectroSpray Ionisation
MS/MS	Mass Spectrometry/Mass Spectrometry (tandem)
MID	Mass Isotopomer Distribution
WB	Western Blot
RNA-Seq	RNA Sequencing

III. Abstract

Pancreatic Ductal Adenocarcinoma (PDAC) is the most frequent neoplasia of the exocrine pancreas with a 5-years overall survival of less than 5% [1]. Poor response to treatments can be attributed, at least in part, to the pervasive heterogeneity of this type of cancer, whose histological differentiation grade ranges from a well differentiated to a poorly differentiated phenotype [2] . My lab previously dissected the transcriptional and epigenetic networks underlying PDAC grading [3]. By using cell line models mimicking different PDAC grades, transcriptional data highlighted an interferon-related signature as peculiar of low-grade PDACs. This project aims at investigating the links between this interferon-related signature and the epithelial phenotype of well-differentiated PDACs. The role of Interferon Regulatory Factor 1 (IRF1), a transcription factor critical for the interferon response, in PDAC differentiation will be investigated. By combining a loss-of-function strategy and RNA-seq this work aimed at defining the targets and the effects of IRF1 differential expression in the mentioned cell line model. Model reliability will also be confirmed via immunohistochemistry on tumour microarrays. The immunological and metabolic phenotypes regulated by IRF1 in well differentiated PDACs will further be analysed by the use of xenografts and cell culture based assays. It will be shown that IRF1 regulates multiple interferon related genes involved in antigen processing and presentation; its deletion affects stromal composition in xenografts. IRF1 deficient cells also rewire their metabolic networks, with changes in lipid composition and metabolite usage. Overall, we found that the transcription factor IRF1 pleiotropically controls a variety of phenotypical traits of low grade PDACs: from antigen processing and presentation pathways, to metabolism, which IRF1 deficiency rewired towards an increased respiratory and lipogenic profile.

IV. Introduction

*IV.1 **Preliminary statement***

Pancreatic Ductal Adenocarcinoma (PDAC) is one of the deadliest forms of cancer worldwide [1] with an outstanding resistance to the most part of currently available therapies [4]. A recent body of work focused at unravelling PDAC heterogeneity [3, 5, 6]: the ultimate goal is to better characterise heterogeneous behaviours and provide novel platforms for therapy development.

The investigations presented in this thesis arise from the observation of an interferon-related signature associated with a high differentiation grade of PDAC cell lines and tumours [3]. I hypothesized that a transcriptional network exclusively expressed in differentiated PDAC cells links the epithelial state to the above-mentioned interferon related signature.

Here, I present my findings on the role of the transcription factor IRF1 (interferon regulatory factor 1) in regulating the Interferon signature in well differentiated PDAC cells. I have investigated the cytological, transcriptional and metabolic phenotypes regulated by IRF1 in well differentiated PDAC cells, and the implications of these results in the biology of pancreatic cancer differentiation. I found that *IRF1* expression is strictly linked to a high grade of differentiation in PDAC cell lines and tumours, and its depletion in well differentiated cells also impacts some epithelial features. Analysis of the transcriptional profile of IRF1-depleted PDAC cells suggest that IRF1 regulates antigen processing and presentation, and directly links a high activity of this pathway to the differentiation grade. These results also provide evidence for a role of IRF1 in the regulation of the metabolic profile of well differentiated PDAC cells.

The following introductory chapter will provide some literature review highlights, with the aim of contextualizing the results and the findings of this work.

IV.2 ***Pancreatic Ductal Adenocarcinoma***

IV.2.1 ***PDAC: an overview***

Pancreatic Ductal Adenocarcinoma (PDAC) is the most common form of pancreatic tumour, accounting for about 85% of cases, and is considered one of the leading causes of cancer-death worldwide [7, 8]. Projected forecasts on its incidence and mortality rates indicate a growing trend worldwide [8, 9]. In spite of substantial efforts in recent decades, PDAC still remains a poorly treatable malignancy with a considerable resilience to therapies. Indeed, no substantial improvement in patients' survival has been obtained in the last 40 years, also in the context of clinical trials for innovative treatments [4].

For the most part, PDACs arise from pancreatic epithelial lesions carrying an activating mutation in the *KRAS* oncogene (in around 30% of early cases and nearly 100% of later stages [1]). *CDKN2A* ($p16^{INK4a}$) loss-of-function by deletion, mutations or promoter methylation; *TP53* loss by inactivating mutations and *SMAD4* inactivation by deletion or mutation represent the most common "second hit" lesions, although other less frequent but common mutations have been identified (*BRCA1*, *BRCA2*, *ARID1A*, *KDM6A*) [1, 10, 11]. In PDAC, tumour initiating events have been classically described as a stepwise progression from precancerous lesions to malignant neoplasms. In the classical model of PDAC tumorigenesis, Acinar to Ductal Metaplasia (ADM) progresses to form Pancreatic Intraepithelial Neoplasia (PanIN), and ultimately PDAC [1, 12]. Alternatively, Intra Papillary Mucinous Neoplasm (IPMN) or Mucinous Cystic Neoplasm

(MCN) may form the precursors of PDAC [1]. It has also been suggested, however, that some PDACs may originate *ex abrupto* from a single series of mitotic catastrophic events [13].

The poor (or partial) responsiveness of this tumour to cytotoxic resulted in a number of PDAC biology studies focusing on inter- and intra-tumoural heterogeneity, as one of the key factors of this resistance [10, 14, 15]. The concept on PDAC heterogeneity paved the way for a number of studies, which tackled the subject from different angles. Recent studies highlighted the genetic [6, 11, 16-18], epigenetic [3, 19], transcriptional [3, 5, 6] and metabolic [20] complexity of this tumour.

From a classical histopathological point of view, PDAC is graded according to the level of differentiation of the tumour cells, from grade 1 (high differentiation) to grade 3 (poor differentiation) [2]. Nevertheless, this appears an oversimplification of a more complex scenario, whereby cells of different grade nearly always coexist in tumour masses [3, 15]. G1 (well differentiated) tumours are formed by well-organized ducts. Epithelial organization is partly lost in G2 tumours, whose papillae show nuclear atypia and incomplete ducts. G3 (poorly differentiated) carcinomas are instead mainly composed of isolated undifferentiated cells or compact cell nests embedded in the tumour stroma [1, 2]. Each of these grades represents an individual grade of differentiation of groups of tumour cells. All the resulting phenotypes may mirror the tumour cell ability to adapt and better fit the constraints of the surrounding environment [10].

To date, attempts at molecular subtyping of pancreatic cancer and pancreatic cancer cells according to their transcriptional profiles mainly described two epithelial subtypes reflecting a high or low degree of differentiation. These two subtypes are named as "*Classical*" and "*Quasi-Mesenchymal*" in Collisson *et al*. [5]; "*Pancreatic*

progenitor" and "*Squamous*" in Bailey *et al.* [6]. Both these work used transcriptional analysis of microdissected tumour samples, in the attempt to isolate the epithelial components. Nonetheless, a refined computation [17] highlighted non-tumour tissue contributions in the profiles defined by Collisson *et al.* [5]; similarly Bailey *et al.* [6] identify an "*Immunogenic*" subtype, closely profiled with "*Pancreatic progenitor*" but severely infiltrated. Cell line models have been used, also to recapitulate and isolate the different phenotypes of PDAC differentiation as in Diaferia *et al.* [3]. Henceforth in this work, the nomenclature will refer to well differentiated PDACs as "*Low grade*" and to poorly differentiated PDACs as "*High grade*" [3].

IV.3 ***PDAC grade and associated molecular phenotypes***

Low or high grade of differentiation in PDACs are associated with the presence of different underlying transcriptional and epigenomic networks [3]. High grade PDACs display a less prominent epithelial phenotype indicated as "*quasi-mesenchymal*" state [5]. They are characterised by the loss of epithelial features, including duct formation *in vivo* and cell-cell adhesive contacts, and by a transcriptional program regulated by the high expression of the transcriptional repressor ZEB1 (Zinc finger E-box-binding homeobox 1), which is directly responsible for suppressing the expression of epithelial identity genes [3, 21]. Low grade PDACs, conversely, exhibit classical epithelial morphology and organisation, including cell-cell junctions and the ability to form ductal epithelia in xenograft models. It has been shown [3] that the maintenance of the epithelial state of these cells is sustained by the activity of epithelial-specific transcription factors (TFs) such as KLF5 (Krüppel Like Factor 5) and ELF3 (E74 Like ETS Transcription Factor 3). Depletion of these grade-specific transcription factors alters the epigenetic and transcriptional profiles of low grade PDAC cells, ultimately leading

to phenotypic changes in the epithelial state. RNA-Seq and chromatin profiling in these cells also highlighted novel TFs as potentially involved in maintenance of differentiation, including FOXA1/2 (Forkhead Box A1/2), HNF1B (Hepatocyte Nuclear Factor 1-beta) and IRF1 (Interferon Regulatory Factor 1).

In addition to the features strictly linked to the epithelial state (e.g. epithelial adhesion molecules), the comparison between low grade and high grade PDAC cell lines highlighted several associated transcriptional signatures selectively enriched in cells of either group. This works focuses on a peculiar interferon-related signature which my lab found as differentially expressed between high grade and low grade PDAC cell lines. Given the relevance of the interferon system in multiple biological processes, including oncogenesis, tumour-immune crosstalk, cell cycle regulation [22, 23], aim of this work is to investigate its impact of the biology of PDACs of different grade.

IV.4 ***Interferons and interferon-related signatures in cancer***

IV.4.1 ***Interferons***

Interferons are a family of cytokines providing a first line of defence against viral infections. In humans, three classes of IFNs are known: type I IFN (IFN-α [-1,-2,-4,-5,-6,-7,-8,-10,-13,-14,-16,-17,-21], IFN-β, IFN-ε, IFN-κ, IFN-ω); type II IFN (IFNγ) and type III IFN (IFN-λ1, - λ2, - λ3) [22]. While type III IFN biology is still a largely unexplored field [24], type I and type II IFNs have been investigated in a number of contexts since their discovery. These two classes act in different pathological contexts, with type I IFN being broadly expressed by nearly all cell types, while type II activity and expression are restricted to some leukocyte lineages [22, 25]. By binding to their type-specific

cell surface receptors, these soluble glycoproteins activate a signalling cascade ultimately leading to the rapid transcriptional induction of a large panel of antiviral molecules. Downstream of the receptors (IFNAR1/R2 for type I, IFNGR1/2 for type II), signalling involves the Janus Kinase family of proteins (JAK1, JAK2, TYK2) and transcription factors of the Signal Transducer and Activator of Transcription family (STATs) [25]. The transcriptional response consists in the expression of the so-called Interferon Stimulated Genes (ISGs), which include proteins with direct antiviral activity (MX Dynamin Like GTPases, MX1/2; 2'-5'-Oligoadenylate Synthetases, OASs; Guanylate Binding Proteins, GBPs) as well as the induction of genes in the antigen processing and presentation pathways [26]. In addition to the antiviral response, it has been shown that IFNs may act as anti-tumour molecules. A constitutive IFN signalling alone is able to prevent cellular transformation in mouse embryonic fibroblasts [23]. Cytostatic and pro-apoptotic effects of IFNs have also been demonstrated in different tumours [22]. Further implications of interferons and interferon-related signatures in cancer therapy will be discussed later in this chapter (section 3.3).

IV.4.2 ***Interferon Regulatory Factors***

Interferon Regulatory Factors are a family of transcription factors, whose first member (IRF1) was initially discovered as an activator of *IFNB* gene expression [27]. Since then, the IRF family has been extended to nine members (IRF1-9), which share a conserved DNA binding domain [28]. Nonetheless, although a conserved Interferon Stimulated Response Element (ISRE) has been described, alternative binding events to the genome, in cooperation with other binding partners, can be found (e.g. the classical STAT1-STAT2-IRF9 complex [25], but also AP1-IRF complexes as in [29-31]). Different IRFs have been widely studied as immune cell regulators as well as essential

transcription factors in immune cell development [28]. Similarly, these transcription factors have also been found to possess pro- or anti-tumorigenic functions [32]. To the aim of this work of thesis, we will review some of the studies which highlighted a role of IRF1 in cancer.

IRF1 has been originally characterised as a tumour suppressor gene by the Taniguchi lab [33], who showed that this transcription factor is able to revert the phenotype of Hras-transformed mouse embryonic fibroblasts [34], as well as to activate *p21* expression upon genotoxic stress, thus phenocopying p53 activity [35]. Moreover, in a non-cancerous injured airway model of epithelial to mesenchymal transition (EMT), it was shown that ZEB1-mediated repression of epithelial traits also suppresses the expression of IRF1, through H3K27me3 deposition at the *IRF1* promoter [36] thus providing a link between EMT and *IRF1* expression itself. It has also been shown that the *IRF1* locus is frequently mutated or deleted in cancer samples, including (but not restricted to), gastric cancer, oesophageal cancer and breast cancer [37-40]. In breast cancer, it has been shown that *IRF1* expression is decreased in more invasive and metastatic cell lines, where it may act as tumour suppressor [41]. In PDAC, two different reports associated a high *IRF1* expression with a higher grade of differentiation [3, 42]. Diaferia *et al.*, additionally, also found IRF1 as part of a low grade PDAC specific cis-regulatory network [3].

IV.4.3 ***Interferon-related signatures in cancer***

Transcriptomics data showed that low grade PDAC cell lines are enriched in an Interferon-related signature [3], meaning that these cells express a set of genes associated with the interferon response. Moreover, their analysis of enriched gene signatures associated with low grade specific hyper-acetylated regulatory regions

retrieved an enrichment of immune-related terms [3]. It is interesting to notice that, although differently annotated, the subtype which has been described by Bailey *et al.* [6] as "*Immunogenic*" shares a close similarity in RNA profiling with the "*Pancreatic progenitor*" subtype, which largely overlaps with the definition of low grade PDACs. Similarly, it was also reported [43] that PDAC samples can be separated in two main subtypes according to the expression of an antiviral response signature. Interestingly, although not stated by the authors, adenovirus mediated lysis sensitive and insensitive cell lines mirror a high grade - low grade separation. In PDACs it has also been shown that the combination of a high IFN signature and a low EMT signature is associated with later recurrence after surgical resection. Conversely, early recurrent tumours showed a low IFN signature and a high EMT signature [44].

Similar reports linking an interferon signature to cancer grade, staging or cancer stem cell-like properties have been described for different types of breast carcinoma [45, 46] and for squamous lung cancer [47]. Doherty *et al.* [45] showed that in triple negative breast cancer, mesenchymal and epithelial subpopulations can be divided based on the interferon gene signature. In breast invasive lobular carcinoma, Michaut *et al.* [46] showed an anti-correlation between EMT signatures and immune-related phenotypes. In squamous lung cell carcinoma, Tong *et al.* [47] showed that Stage II/III samples downregulated the interferon-related signature to levels comparable to those of Stage I samples.

IFN-related signatures have also been described as markers of prognosis or therapeutic response. A high Interferon Related DNA damage Resistance signature (IRDS) has been described as a prognostic marker for the resistance to genotoxic therapies, including radiation therapy [48]. IRDS separates two discrete populations across multiple cancer types (head and neck, breast, prostate, lung, glioma) [48].

Concordantly with this data, Sistigu *et al.* [49] showed in mouse models and breast cancer patients, that functional type I IFN signalling is necessary to elicit a response to anthracyclines, with a cancer cell-autonomous contribution to chemosensitivity [49]. IFN stimulation also chemo-sensitises melanoma cell lines to inhibition of the protein kinase MEK, which is part of the ERK pathway. Nonetheless the effect could be achieved only in cells with a low basal level of IFN signature, while cell lines high in this signature were resistant to MEK inhibition [50]. To date, interferons, interferon stimulated genes and their potential in cancer therapy are an open subject of investigations with obvious practical implications [22].

IV.5 ***PDAC metabolism***

PDAC metabolism is, to a large extent, governed by the impact of KRAS activation, the most common mutation in this type of cancer [51]. The constitutive activation of this oncogene drives a hyper-proliferative program via the activation of a number of downstream signalling pathways. Thus, *KRAS* mutant cells have to meet the metabolic needs of this increased proliferation rate by altering their metabolic profile [51]. KRAS mutation in PDAC has been linked to different metabolic programs (Fig. 1). In an inducible $KRAS^{G12D}$ mouse model of PDAC, it has been shown that KRAS mutation is able to enhance glycolysis but it does not affect TCA cycle. Moreover, this mutation is linked to enhanced glucose carbons usage in the hexosamine pathway, which controls the synthesis of the glycan precursor of glycoproteins, and in the pentose phosphate pathway, which controls the synthesis of ribose as nucleobase precursor [52]. Additionally, also glutamine usage pathways are rewired upon KRAS mutation in PDAC. This mutation, in fact, inhibits the activity of the oxidative pathway from glutamine to α-ketoglutarate (which replenishes α-ketoglutarate levels in the TCA cycle), while it

promotes the glutamate transaminase-mediated pathway for the ultimate conversion of oxaloacetate to pyruvate and increased activity of NADPH producing Malic Enzyme 1 (ME1) (Fig. 1) [53]. NADPH production by ME1 has been shown to be essential for PDAC cell survival, while ME2 and ME3 isoforms appeared to be redundantly linked to ROS scavenging and pro-survival routes [54].

Lipid metabolism is also rerouted during PDAC development. Whole-tumour metabolomics showed an enriched fatty acid related network relative to the normal pancreatic tissue [55]. In a genetically engineered mouse model of PDAC, it has been shown that cholesterol uptake is strongly increased in cancerous lesions, and the disruption of this pathway can slow down cancer proliferation [56].

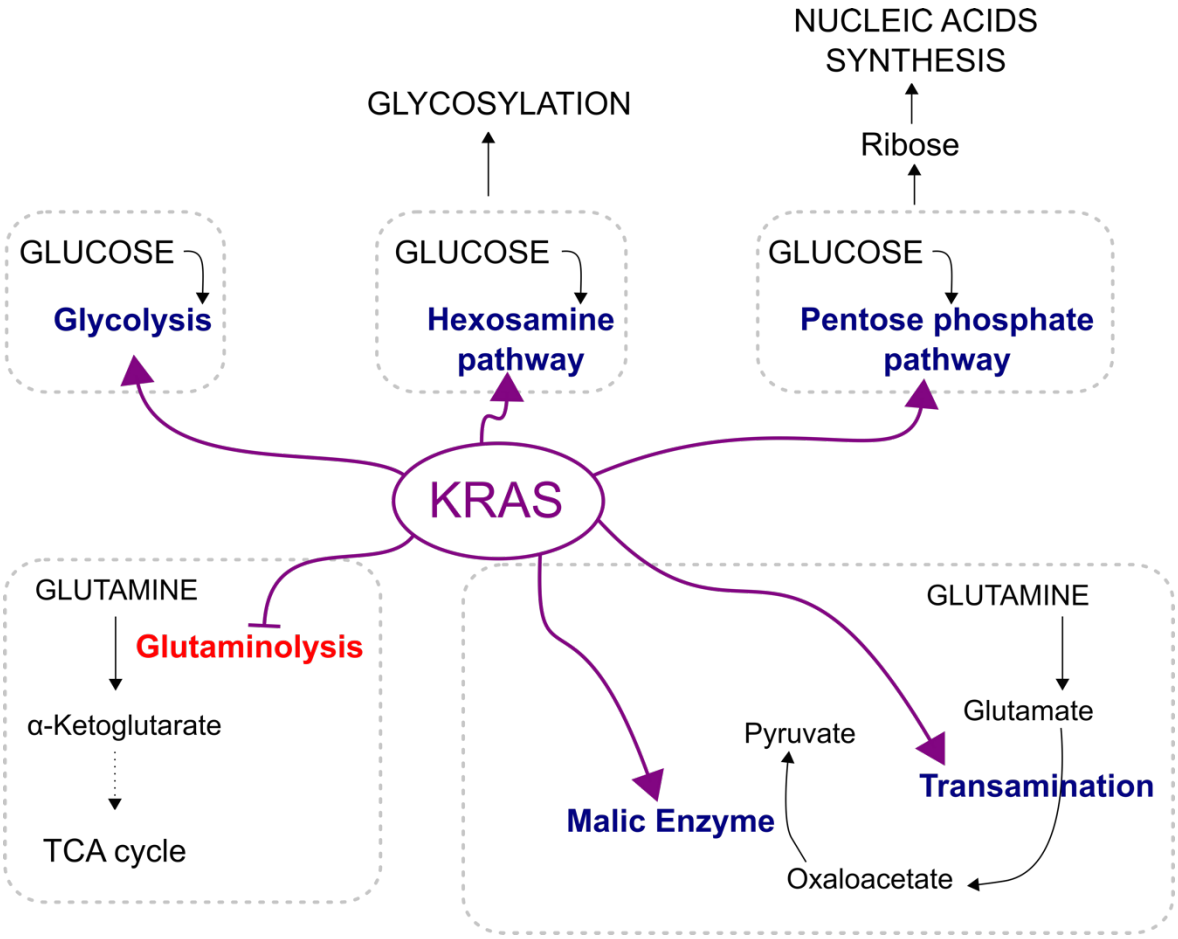

Figure 1: Metabolic consequences of KRAS activating mutations in PDAC

Schematic view of KRAS induced metabolic changes described in PDAC [51]. Hyperactivated pathways are shown in blue (Glycolysis [52], Hexosamine pathway [52], Pentose phosphate pathway [52], Glutamate transamination [53], Oxaloacetate

decarboxylation by malic enzymes [53] [54]). KRAS mutation inhibits Glutaminolysis [53].

In this scenario, attempts have also been made to investigate the metabolic heterogeneity of PDAC. Distant metastases of pancreatic cancers, for example, have been shown to be epigenetically reprogrammed –as compared to the tumour of origin– to increase their dependence from the pentose phosphate pathway. Conversely, the inhibition of this pathway could reverse the acquired epigenetic programs, thus reversing the transcriptional programs of these cells [57]. Differential activation of metabolic pathways has also been linked to oxygen availability to PDAC cells: it has been shown that hypoxia can increase the activity of the hexosamine pathway in PDACs, while inducing a more mesenchymal phenotype of tumours [58]. Nonetheless, normoxic and more epithelial tumours showed the ability to use lactate as a carbon source, while hypoxic ones could not [59]. Daemen *et al.* [20] attempted a metabolic stratification of PDACs by using a vast panel of PDAC cell lines. Three metabolic subtypes were identified: a lipogenic subtype, showing a distinct enrichment for lipids and lipogenic enzymes, a glycolytic subtype, strongly dependent on glycolysis, and a slow proliferating subtype, with an intermediate lipogenic and glycolytic profile that was low in aminoacid and carbohydrate content. Interestingly, when compared to the molecular subtyping by Collisson *et al.* [5], the lipogenic and glycolytic subtypes mirrored –respectively– the "*epithelial*" and the "*quasi-mesenchymal*" subtypes. These observations suggest the possibility that differentiation grade in PDAC also impacts metabolic properties.

V. Results

V.1 ***The differential expression of the interferon-related signature is not associated with type I IFN locus mutations***

Pancreatic cancer cell lines often bear extensive alterations of the chromosomal region 9p21.3, including frequent co-deletion events of *CDKN2A* and the type I IFN gene cluster [60]. Therefore, the association between the interferon-related signature of low grade PDAC cells and status of the type I IFN locus was investigated. PCR primers were designed to amplify multiple regions of the locus. Two probes designed 1 Mbp upstream and downstream of this genomic region (including *CDKN2A* locus, Fig. 2a-b) were also designed. As WT control the genomic DNA from an immortalized human pancreatic ductal epithelium cell line was used. No association between the mutational status of the locus and cell line grade could be observed. Indeed, both groups of cells showed a heterogeneous mutational landscape, ranging from the complete deletion (CAPAN1, MiaPaca2) to the maintenance of a wild type locus (CFPAC1, PANC1), irrespective of cell line grade (Fig. 2c).

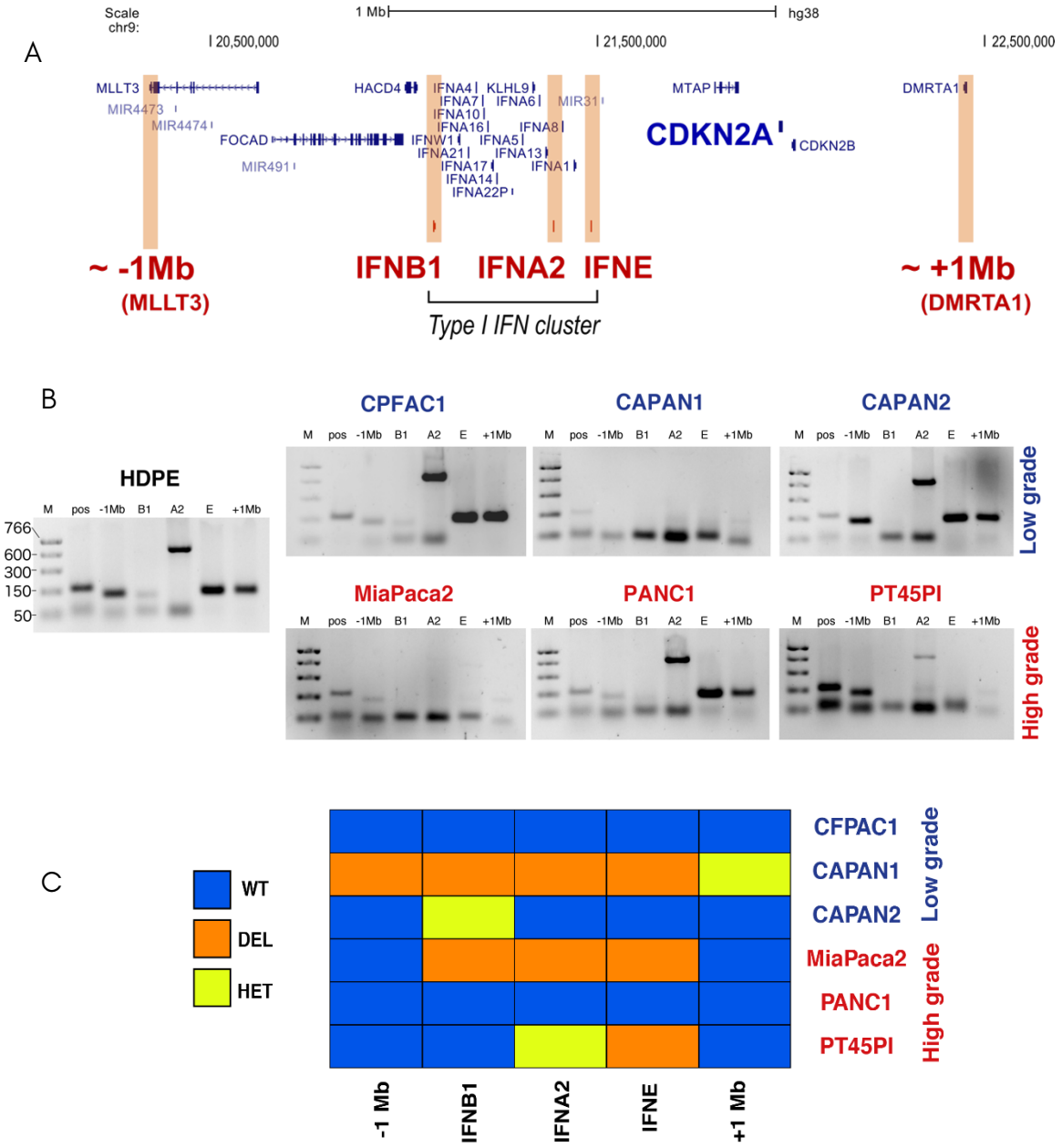

Figure 2: Mutation of the IFN locus in PDAC cell lines

A) Type I IFN cluster of genes. Scheme of 9p21.3 region of the genome. Highlighted in red and orange, the genes in which regions were selected as probes for the mutational assessment of the region. Type I IFN cluster of genes. Scheme of 9p21.3 region of the genome. Highlighted in red and orange, the genes in which regions were selected as probes for the mutational assessment of the region.

B) PCR for the assessment of the mutations in Type I IFN cluster. HDPE: Human Pancreatic Ductal Epithelium cell line. Low grade cell lines are shown in blue (CFPAC1, CAPAN1, CAPAN2), high grade cell lines in red (MiaPaca2, PANC1, PT45PI). M: Marker, pos: positive PCR control (GAPDH promoter), B1: IFNB1, A2: IFNA2, E: IFNE. Expected sizes: pos: 166 bp; -1Mb:149 bp; IFNB1: 137 bp; IFNA2: 555 bp; IFNE: 144 bp; +1Mb: 146 bp

C) Heatmap summarizing the PCR results: rows: cell lines. Low grade cell lines in blue (CFPAC1, CAPAN1, CAPAN2), high grade cell lines in red (MiaPaca2, PANC1, PT45PI); columns: probes. Light blue: WT locus; Orange: deleted locus; Yellow: partial deletion/multiple bands.

V.2 ***PDAC cell lines show similar activation of the IFN signalling cascade, but differ in transcriptional response***

To explore the interferon signature in PDAC cell lines, differential expression data from previous RNA-Seq experiments generated in the lab [3] were analysed, in order to determine whether the differential activation of the pathway was related to differential expression of some member of the interferon signalling cascade. Unsupervised hierarchical clustering of expression data for the main effectors of the early signalling cascade (IFN receptors *IFNAR1*, *IFNAR2*, *IFNGR*; Signal Transducer and Activator of Transcription *STAT1* and *STAT2*; Janus Kinases *JAK1*, *JAK2* and *TYK2*), however, showed no clustering between high grade and low grade cell lines (Fig. 3).

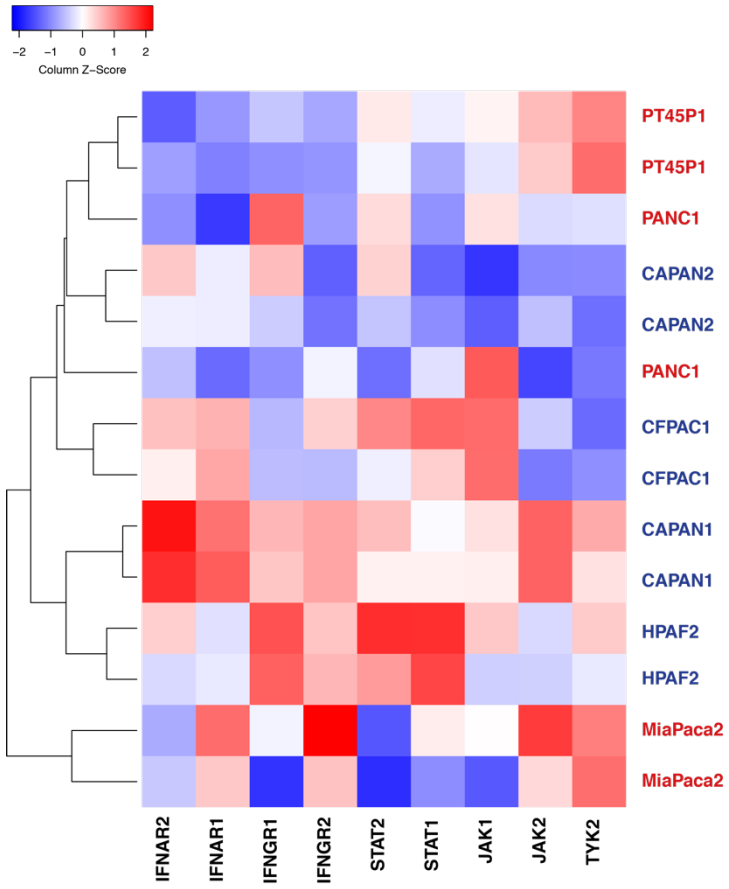

Figure 3: Heatmap of expression data of the main effectors of the IFN signaling cascade in PDAC cell lines.

Unsupervised hierarchical clustering shows no clustering between cell line grade and expression of signaling molecules. Low grade cell lines in blue (CFPAC1, CAPAN1, CAPAN2), high grade cell lines in red (MiaPaca2, PANC1, PT45PI).

To further confirm these data, PDAC cell lines were treated with human Interferon β and the activation of the signalling cascade was assayed via Western blot analysis and quantitative PCR (Fig. 4a). Following 2 hours of treatment, all cell lines displayed activation of the signalling cascade, as measured by the levels of phosphorylated STAT1 (pSTAT1-Y701). The mRNA levels were detected by qPCR of classical ISGs (*GBP2*, *MX1*, *IRF1*) (Fig. 4b) and revealed a higher activation of the transcriptional response upon IFNβ treatment in low grade cell lines compared to high grade cell lines. Together, these data suggest that low grade and high grade PDAC cell lines can similarly activate the interferon signalling cascade, but the transcriptional activation of ISGs is higher in low grade PDAC cells.

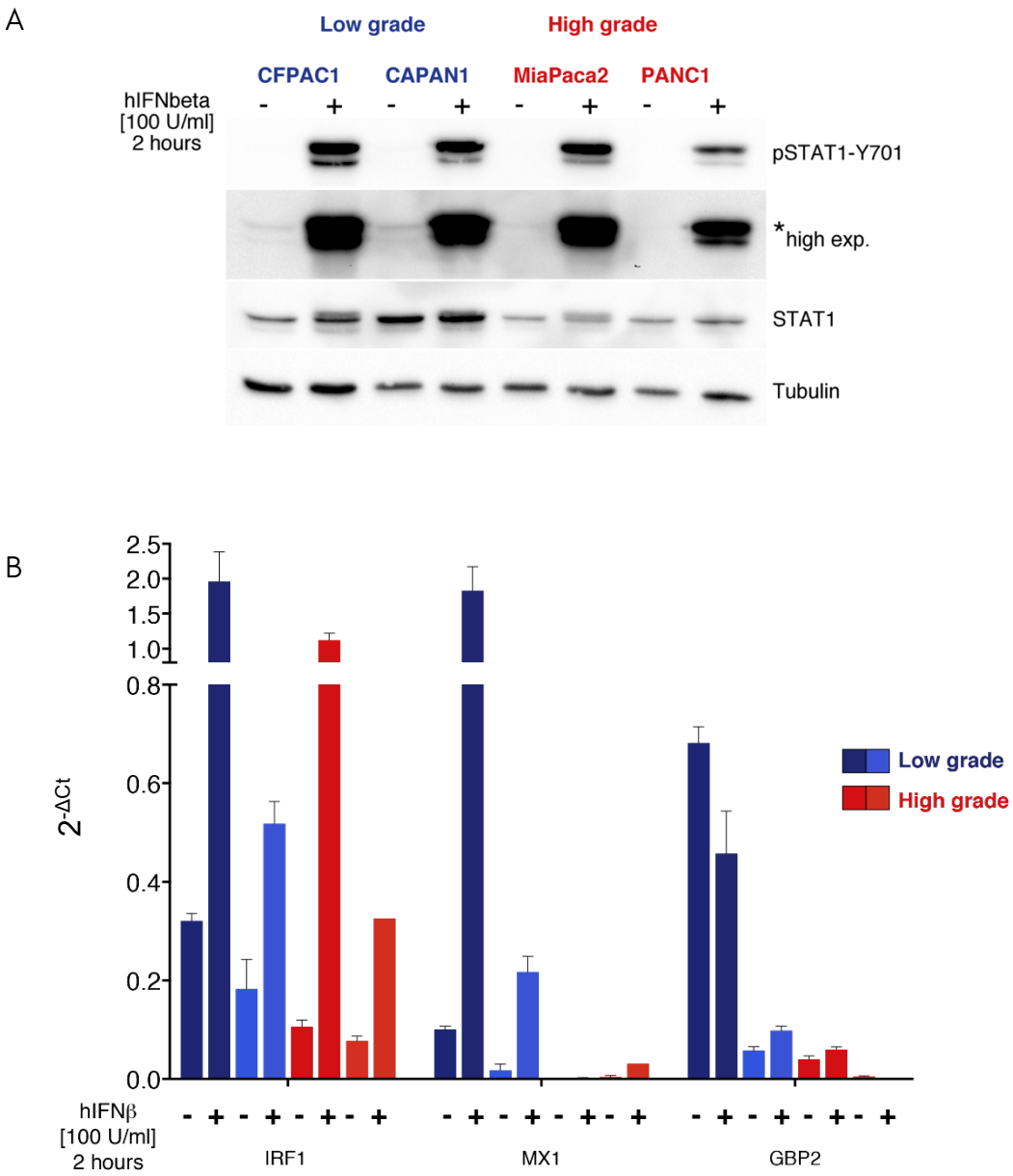

Figure 4: Signalling and transcriptional response to IFN stimulus in PDAC cell lines

A) Interferon stimulation on pancreatic cancer cell lines initiates the signalling cascade irrespective of cell line grade. Western analysis of STAT1 phosphorylation on Tyrosine701 (Y701) and total STAT1 in PDAC cell lines, untreated and after 2 hours of IFNβ stimulation (100 U/ml). Low grade cell lines in blue (CFPAC1, CAPAN1), high grade cell lines in red (MiaPaca2, PANC1). Tubulin is shown as a loading control. *high exp: high exposure is shown to highlight basal pSTA1-Y701 levels in low grade cell lines.

B) qPCR of ISGs on PDAC cell lines, untreated and after 2 hours of IFNβ stimulation at 100 U/ml concentration shows the different transcriptional response of high grade and low grade cell lines to IFN stimulus. Low grade cell lines in blue (dark, CFPAC1; light, CAPAN1), high grade cell lines in red (dark, MiaPaca2; light, PANC1).

V.3 *IRF1 is differentially expressed between high grade and low grade PDAC cell lines and tumours*

As shown before, the interferon-related signature of low grade PDAC cells was not associated with either type I IFN locus deletion nor with discrepancies in the signalling events. Therefore, a role for cell type-specific transcriptional networks in the maintenance of the signature was hypothesized. Previously published datasets [3] showed differential expression of *IRF1* between high grade and low grade PDAC cell lines; as well as the enrichment of the IRF1 binding motif in low grade specific hyper-acetylated genomic regions [3]. This differential expression was further confirmed by Western blot analysis in lysates from PDAC cell lines (Fig. 5) and immunohistochemistry on human PDACs. The percentage of anti-IRF1 immuno-reactive tumour cells on a tissue microarray of human PDAC samples was measured (Fig. 6a). Within each sample, the histological grade of individual groups of tumour cells was assessed (Grade 1 to 3). Grade 1 tumour areas (n=45) showed a significant enrichment in IRF1 positivity compared both to Grade 2 (n=42) and Grade 3 (n=164) areas (unpaired Welch's t-test, p=0,0186 and p<0,0001 respectively). These data showed that IRF1 is differentially expressed in areas of human PDACs with distinct grade of differentiation.

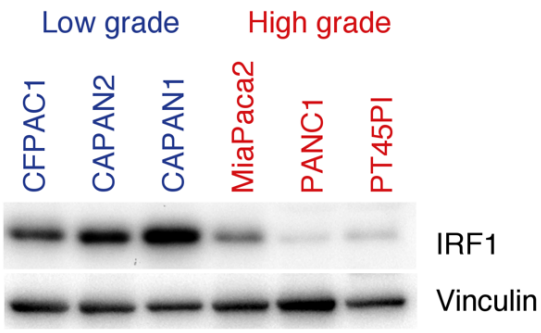

Figure 5: Expression of IRF1 in different human PDAC cell lines.

WB showing the expression of IRF1 in PDAC cell lines. Vinculin is shown as loading control. Low grade cell lines are shown in blue (CFPAC1, CAPAN1, CAPAN2), high grade cell lines in red (MiaPaca2, PANC1, PT45PI).

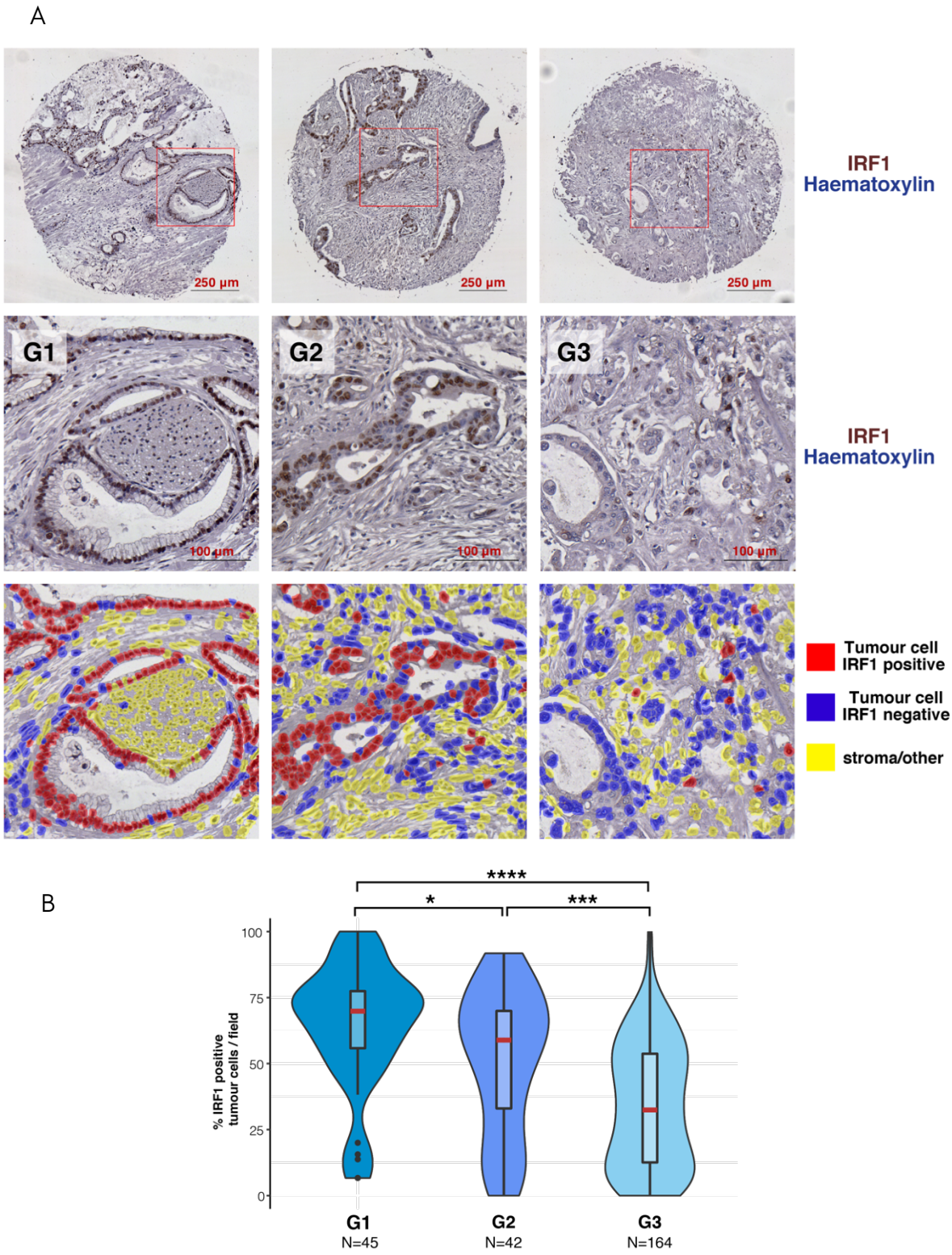

Figure 6: IRF1 immunoreactivity of human pancreatic cancers according to tumour grade

A) Rows 1-2: Representative IRF1 immunohistochemistry of human tumours. Grade 1 to Grade 3 tumour samples are shown. Positive cells are brown (DAB), haematoxylin (blue) as counterstain. Row 3: Pseudocolor segmented images of Row 2 samples. Red for IRF1 positive cells, blue for negative tumour cells, yellow for non-tumour cells.

B) Violin plot of IRF1 positive tumour cells percentage per field, divided by local histological grade. Medians highlighted in red. G1 vs G3: * p=0,0186; G2 vs G3: ***p=0,0004; G1 vs G3: **** p<0,0001; unpaired Welch's t-test.

V.4 *IRF1-deficient low grade cells display aberrant cell shape, motility and adhesion*

To evaluate the role of IRF1 in differentiated PDAC cells, CRISPR-Cas9 technology was used to knock it out in a low grade cell line, CFPAC1 (Fig. 7). IRF1-KO and WT (infected with empty Cas9 vector) clones were isolated. Isolated KO clones displayed a loss of epithelial phenotype, growing in an elongated and isolated fashion rather than packed in epithelial clusters (Fig. 8a). IRF1-KO clones, indeed, showed a significantly different circularity index compared to WT clones (Fig. 8b, unpaired Student's t-test, p <0,0001). To further corroborate this observation, other epithelial traits in IRF1-deficient low grade cells were assayed. IRF1 deletion significantly decreased the adhesion of CFPAC1 cells on laminin and poly-Lysine (unpaired Student's t-test, p=0,0002 and p=0,041 respectively), although a similar trend in decreased adhesion can be observed on other matrixes (collagen, matrigel, fibronectin) (Fig. 9). Changes in motility could be observed by comparing random migration paths of WT and IRF1-KO cells (Fig. 10a-b). IRF1-deficient cells decreased their ability to form epithelioid clusters over time and cell-cell adhesion events were reduced. Cell motility parameters were measured (Fig. 10a-b). Although no changes in either length of the path covered within 24 hours or in cell velocity were observed, a significant change in the directionality was measured (unpaired Welch's t-test, p=0,0209). These data showed that IRF1 deletion leads to a partial alteration of epithelial properties in low grade PDACs.

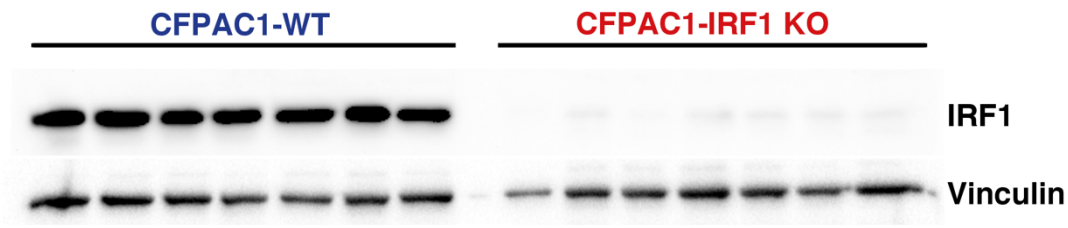

Figure 7: Western blot of IRF1 in IRF1 WT clones of CFPAC1 cell line and IRF1-KO clones. Vinculin is shown as a loading control.

A

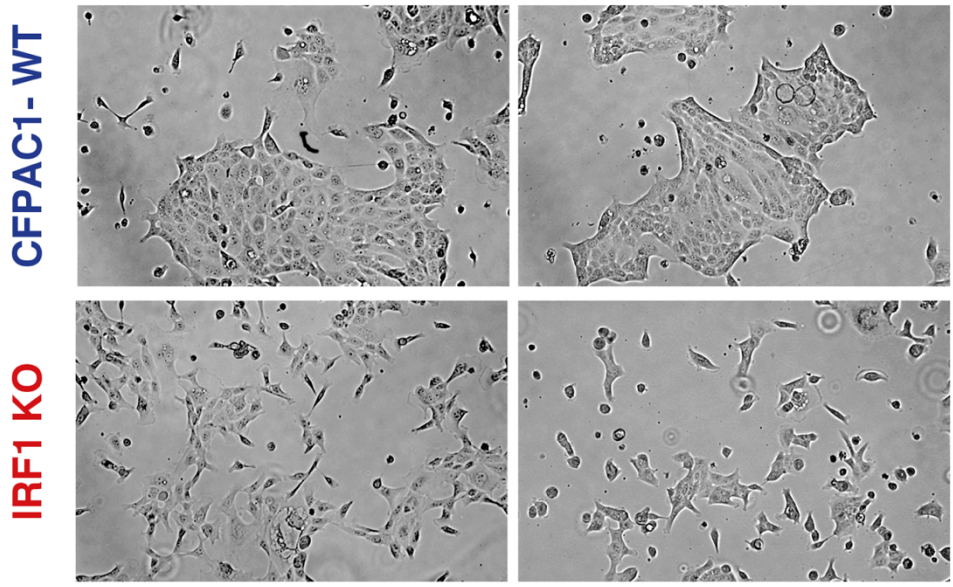

B

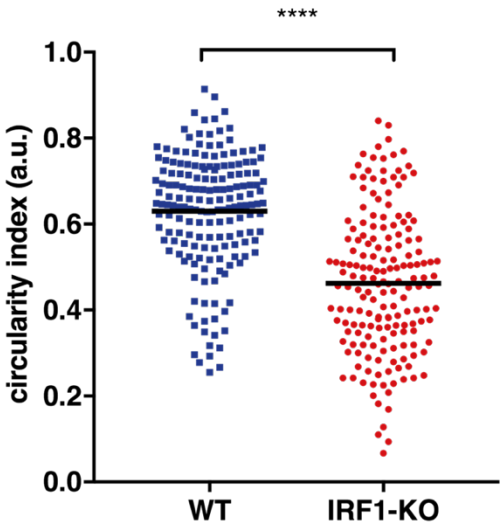

Figure 8: Epithelial traits of WT and IRF1-KO CFPAC1 cells: cell shape and circularity

A) Representative images of two WT (top row) and two IRF1-KO clones (bottom row).

B) Dot plot of circularity index for WT (blue) and IRF1-KO (red) cells. Mean is shown in black. unpaired Student's t-test, **** p <0,0001.

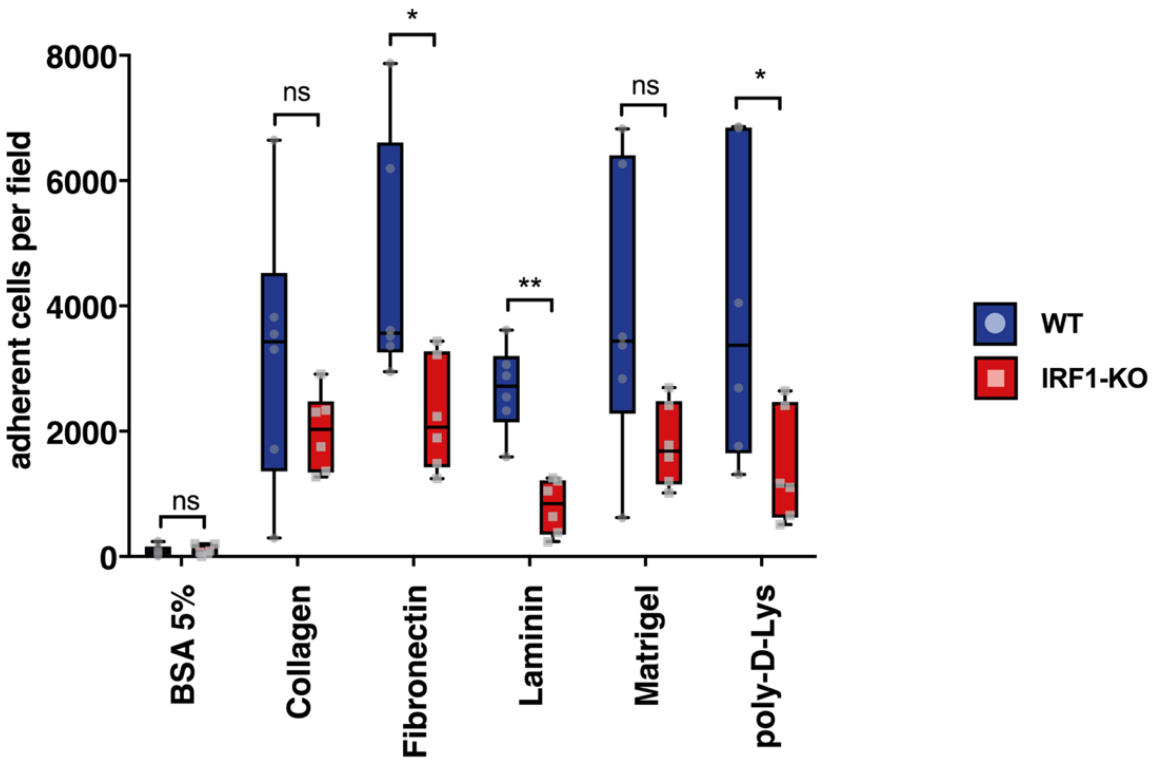

Figure 9: Adhesion of WT and IRF1-KO CFPAC1 cells on different matrixes

Box plot of adherent cells per field on different matrices. Fibronectin, * p= 0,0255; laminin, ** p= 0,0002, poly-D-Lysine * p= 0,0410; unpaired Student's t-test.

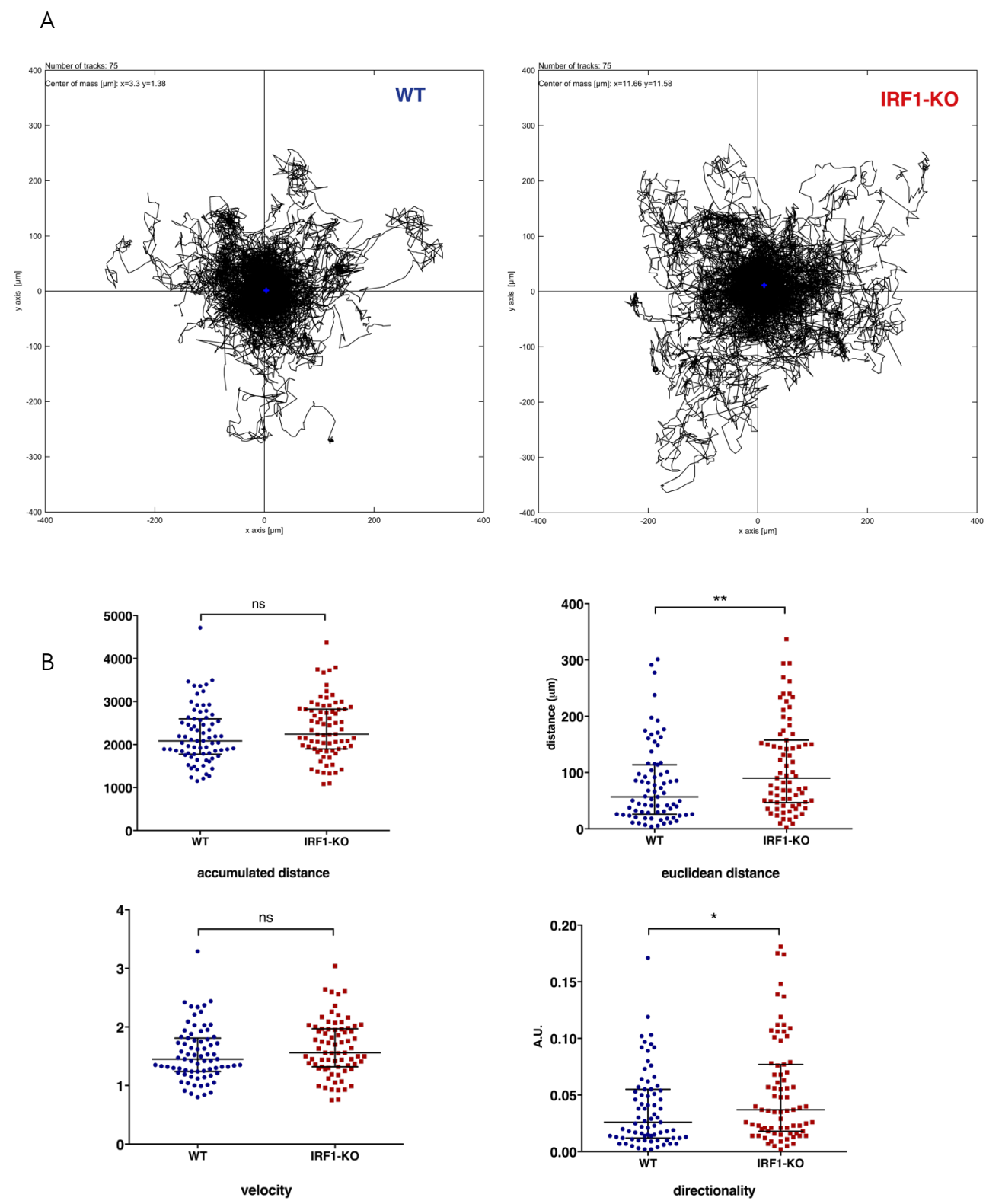

Figure 10: Motility paths and parameters of WT and IRF1-KO CFPAC1 cells

A) Trajectory plots for WT (left) and IRF1-KO (right) cells over a 24 hours time-lapse. Plots are centred on the (0,0) coordinate. Centre of mass of all trajectories overlap is shown in blue.

B) Dot-plots of motility indexes of WT (blue) and IRF1-KO (red) cells. Mean and IQR are shown. Directionality: * p=0,0209; Euclidean distance: ** p=0,0100; unpaired Welch's t-test.

V.5 ***IRF1 deletion affects cell growth rate and stromal components density in mouse xenografts***

The impact of the changes in epithelial phenotype on the overall growth rate of IRF1 deficient cells was assayed. When grown in vitro, little albeit significant differences were observed in growth rates of WT and IRF1-KO clones (p=0,0338, Two-way ANOVA, Fig. 11a). A bigger difference was observed, however, when a pool of the same clones was subcutaneously xenotransplanted in nude mice, with IRF1 deficient cells forming bigger tumours compared to WT (p=0,0072, Two-way ANOVA, Fig. 11b).

Staining of WT and IRF1-KO xenotransplants showed no macroscopic differences in tumour duct formation (Fig. 11c). Instead, a difference in density of the stromal compartment was visible. Some general components of the stroma including, murine macrophage infiltration (IBA1 positive cells) and collagen deposition (Picrosirius Red-positive fibres) were measured. Both collagen fibres (Fig. 12a-b, p=0,0024, Unpaired Student's T-test) and macrophage infiltration (Fig. 12c-d, p<0,0001, Unpaired Student's T-test) were significantly decreased in IRF1-KO tumours. Strikingly, macrophage infiltration of the latter reached levels comparable to the ones of high-grade cells xenotransplants (Fig. 12d-e). Altogether, these data suggest that IRF1 expression in PDAC cells modulates the crosstalk with the stromal compartments.

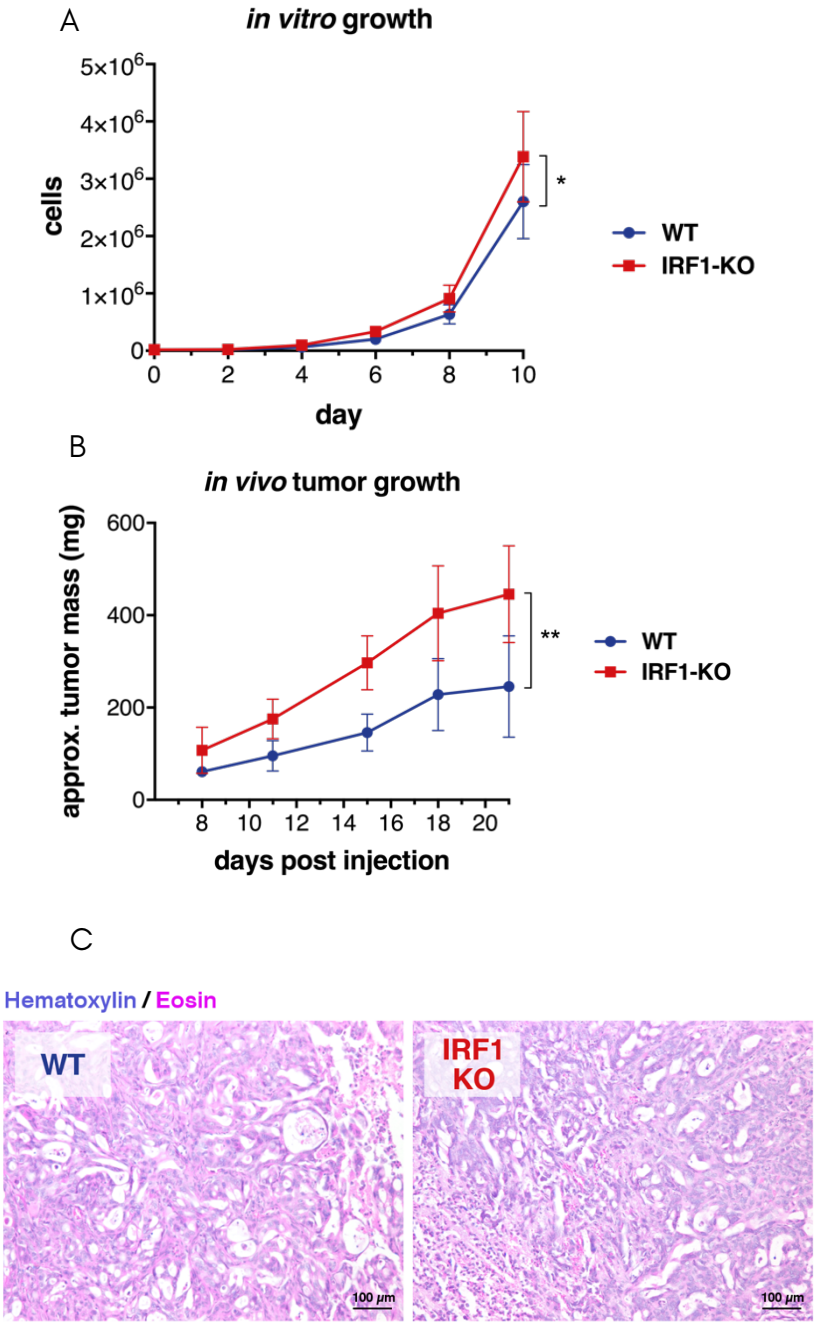

Figure 11: Effects of IRF1 deletion on *in vitro* and *in vivo* growth rates of CPFAC1 cells

A) Cumulative growth curves for WT (blue) and IRF1-KO clones (red). * p=0,0338, Two-way ANOVA.

B) Xenografts growth curves (approximate tumour mass in mg *vs* days post injection). WT (blue) and IRF1-KO clones (red). ** p=0,0072, Two-way ANOVA.

C) H&E of WT(left) and IRF1-KO (right) CFPAC1 xenografts.

A

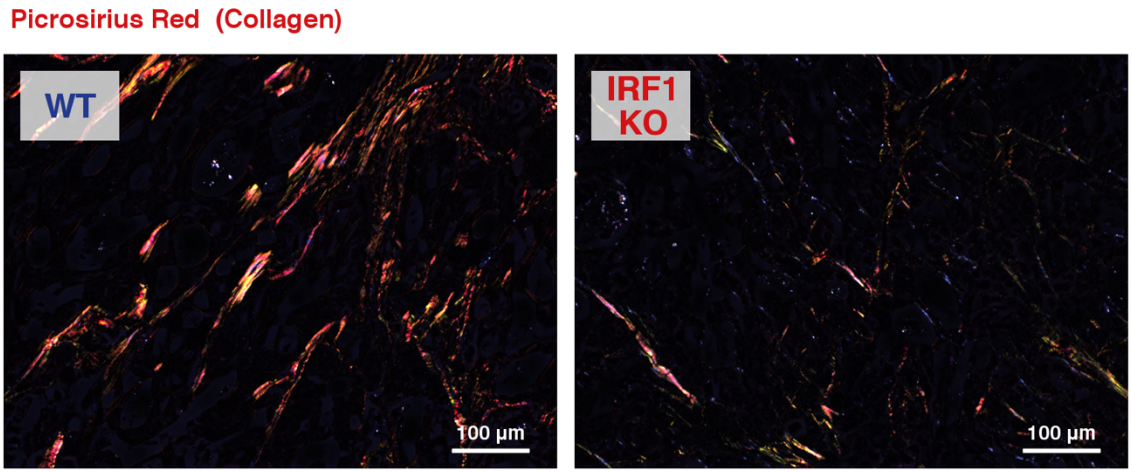

B

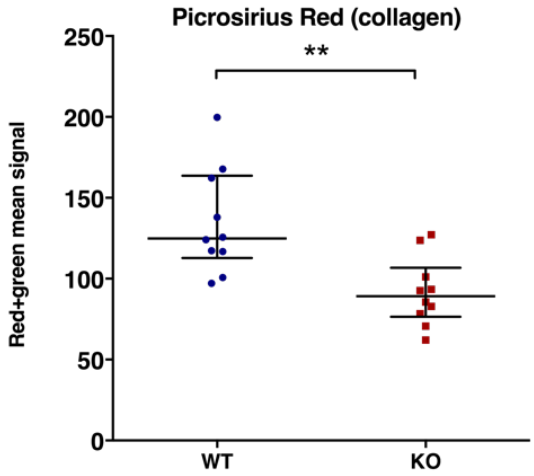

(Fig.12: continues to next page)

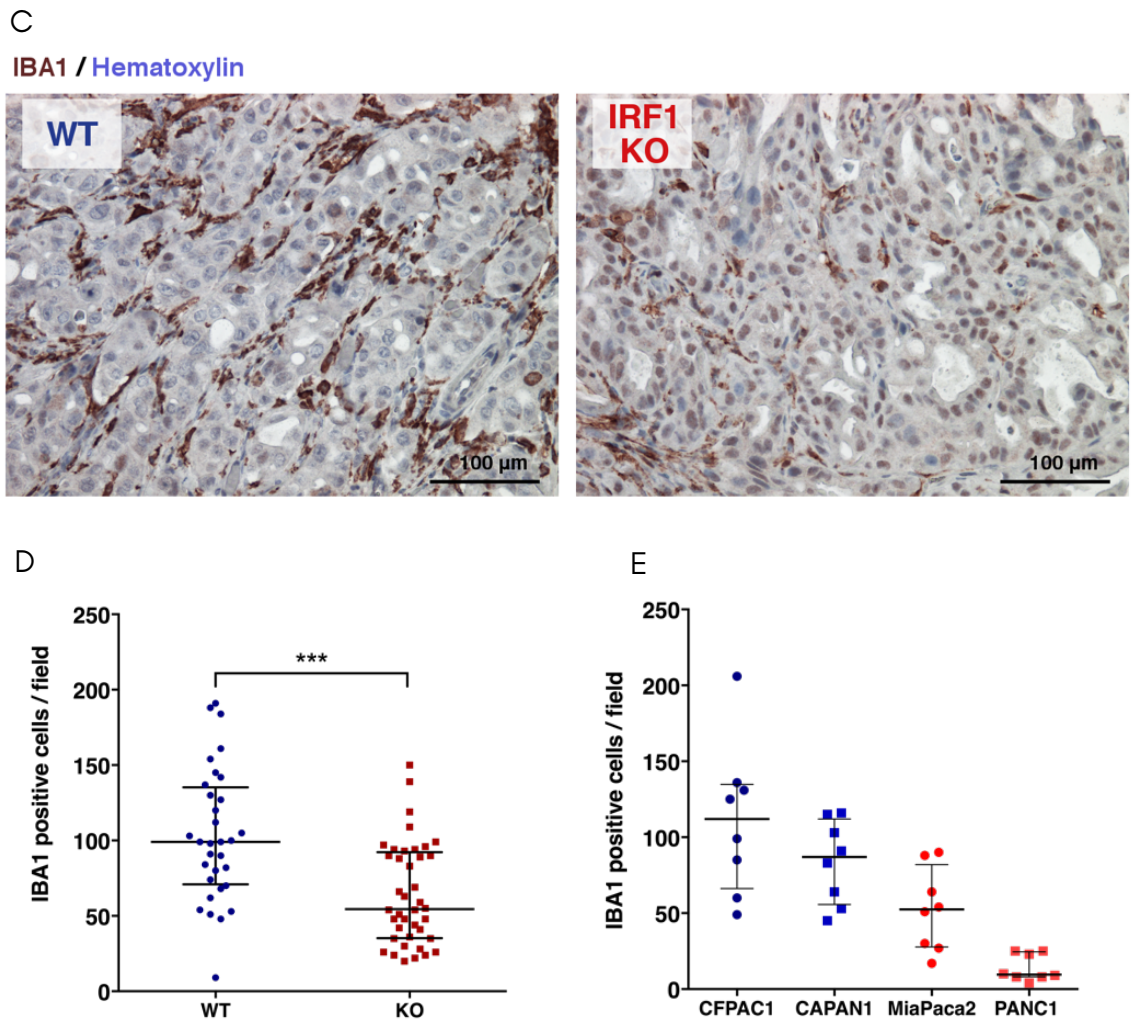

Figure 12: Stromal composition alteration in CFPAC1 xenografts upon IRF1 deletion

A) Polarized light microscopy of Picrosirius Red staining of collagen fibres in WT (left) and IRF1-KO (right) CFPAC1 xenografts.

B) Dot plot: Picrosirius red quantification in WT (left) and IRF1-KO (red + green pixel mean signal, arbitrary units). ** p=0,0024, Unpaired Student's T-test.

C) IBA1 immunohistochemistry of murine macrophages in WT(left) and IRF1-KO (right) CFPAC1 xenografts.

D) Dot plot: IBA1 positive cells per field in WT (left) and IRF1-KO. *** p<0,0001, Unpaired Student's T-test.

E) Dot plot: IBA1 positive cells per field in low grade (blue) and high grade (red) cells.

V.6 ***Transcriptomic profile of IRF1-KO low grade cells***

To investigate the general remodelling of the transcriptional profile upon IRF1 deletion in low grade PDAC cells, IRF1-KO and WT clones were analysed by RNA-Seq. 122 transcripts were significantly deregulated in the WT vs IRF1-KO comparison (log_2Fold Change ≥ |0.70| and False Discovery Rate (FDR) < 0.05 and at least 3 TPM (Transcripts Per Million) in at least 3 samples in each condition) (Fig. 13). 72 transcripts were downregulated, while 50 transcripts were upregulated.

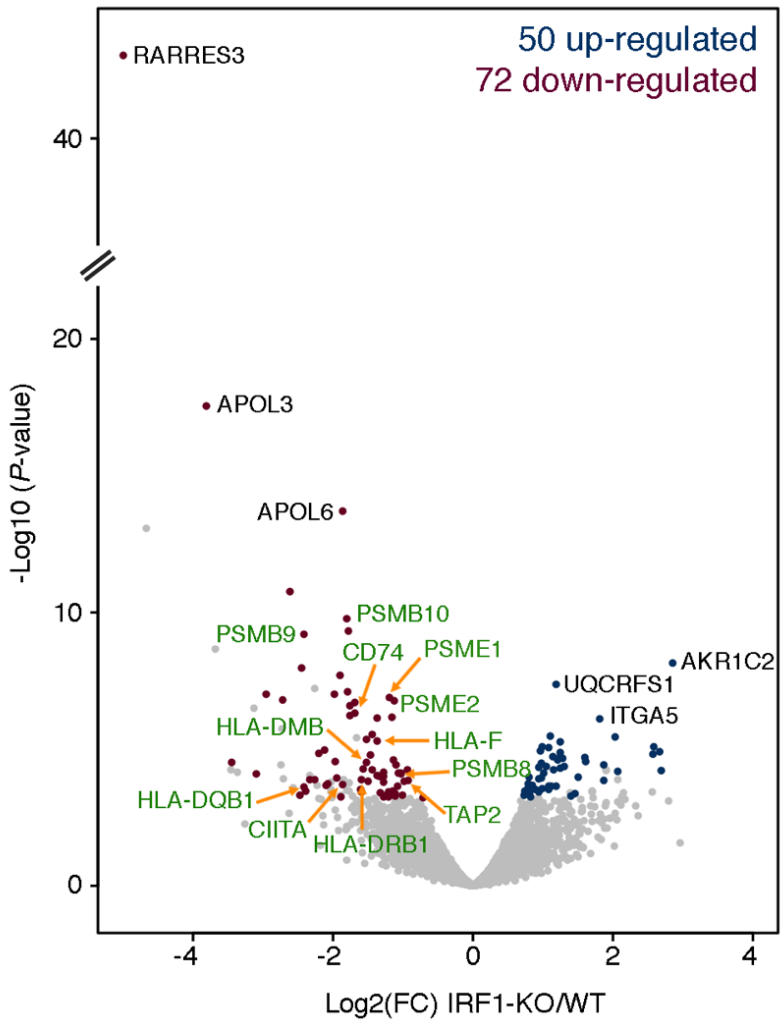

Figure 13: Volcano plot of differentially expressed genes from RNA-Seq of IRF1-KO vs WT CFPAC1 cells.

Downregulated transcripts on the left, upregulated transcripts on the right. Highlighted in green the transcripts related to the antigen processing and presentation pathways.

To gain further insight into the overall behaviour of IRF1-KO cells, a Gene Ontology (GO) annotation using DAVID [61] on differentially expressed genes (DEGs) was run (Fig. 14). GO terms that were downregulated upon IRF1 deletion pre-eminently showed a direct role of this transcription factor on the regulation of the antigen processing and presentation pathways and on interferon-related signatures (e.g. *interferon-gamma-mediated signalling pathway; antigen processing and presentation; type I interferon signalling pathway; etc.*). A second pattern of annotations showed an enrichment for metabolism-related terms associated to lipid metabolism and oxidation-reduction (e.g. Upregulated: *cholesterol biosynthetic process; lipoprotein metabolic process; lipid transport*; *etc.;* Downregulated: *oxidation-reduction process; cell redox homeostasis; electron carrier activity; etc.*).

Similar results were obtained using another functional annotation method, Gene Set Enrichment Analysis (GSEA) [62], which retrieved a significant enrichment of annotated Interferon-related signatures as downregulated in IRF1-KO cells compared to WT (Fig. 15).

Figure 14: (next page) Gene Ontology enrichment analysis of deregulated genes in IRF1-KO CFPAC1 *vs* WT CFPAC1

GO annotation highlights the downregulation of interferon- and inflammation-related signatures, as well as a general metabolic rewiring.

GO annotations from DAVID were visualized using ReVIGO. $-\log_{10}$ (p-value) is colour coded (see in-figure legend). GO enrichment size is plotted as the size of individual bubbles.

Biological Process (column 1), Cellular Component (column 2) and Molecular Function (column 3) ontologies are shown separately. Top row: Downregulated ontologies in IRF1-KO cells; Bottom row: Upregulated ontologies in IRF1-KO cells.

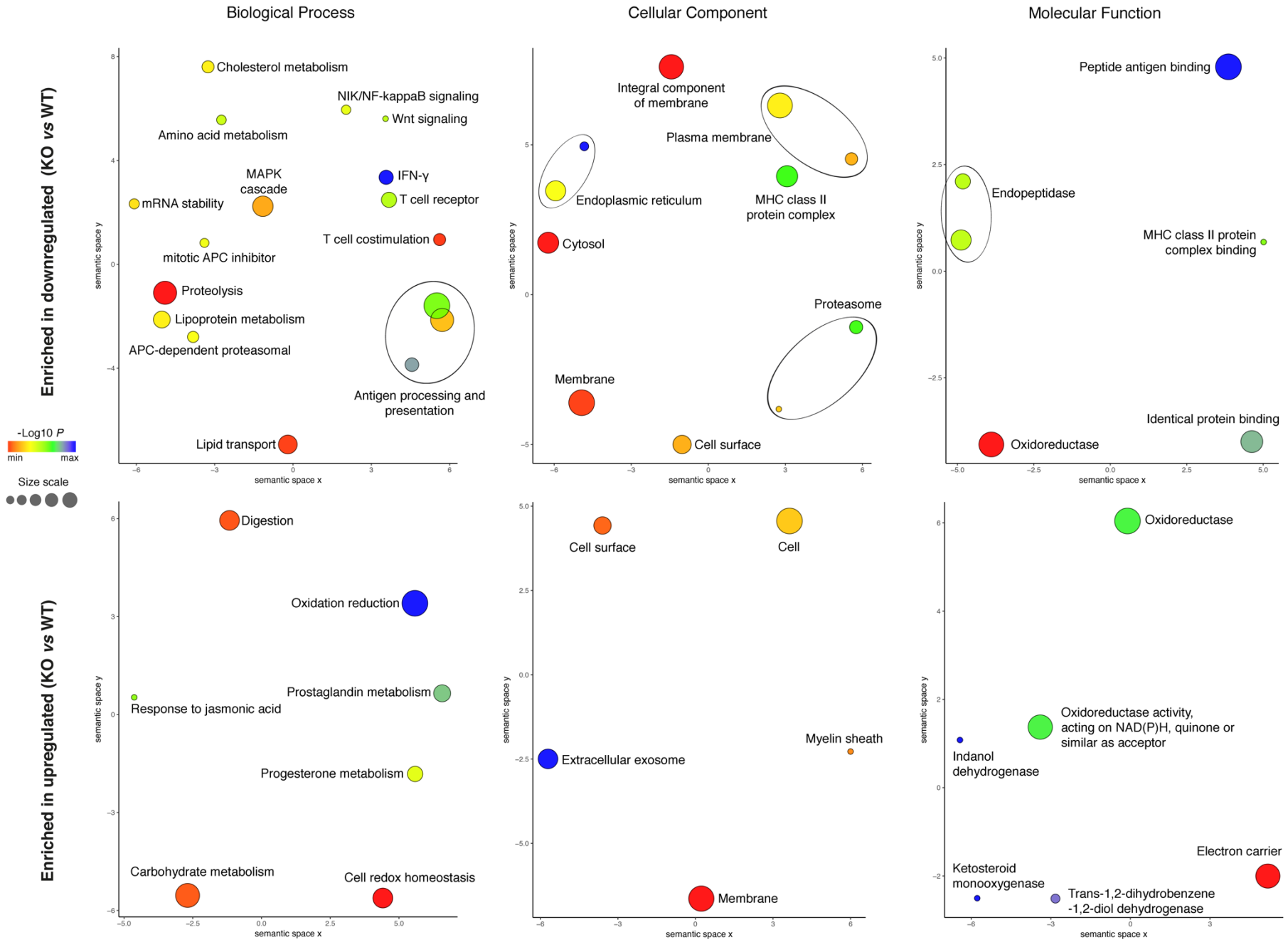
Biological Process
Cellular Component
Molecular Function
Enriched in downregulated (KO vs WT)
Enriched in upregulated (KO vs WT)
-Log10 P
min
max
Size scale
Cholesterol metabolism
NIK/NF-kappaB signaling
Wnt signaling
Amino acid metabolism
MAPK cascade
IFN-γ
T cell receptor
mRNA stability
T cell costimulation
mitotic APC inhibitor
Proteolysis
Lipoprotein metabolism
APC-dependent proteasomal
Antigen processing and presentation
Lipid transport
Integral component of membrane
Plasma membrane
Endoplasmic reticulum
MHC class II protein complex
Cytosol
Proteasome
Membrane
Cell surface
Peptide antigen binding
Endopeptidase
MHC class II protein complex binding
Identical protein binding
Oxidoreductase
Digestion
Oxidation reduction
Prostaglandin metabolism
Response to jasmonic acid
Progesterone metabolism
Carbohydrate metabolism
Cell redox homeostasis
Cell surface
Cell
Extracellular exosome
Myelin sheath
Membrane
Oxidoreductase
Oxidoreductase activity, acting on NAD(P)H, quinone or similar as acceptor
Indanol dehydrogenase
Electron carrier
Ketosteroid monooxygenase
Trans-1,2-dihydrobenzene -1,2-diol dehydrogenase
semantic space x
semantic space y

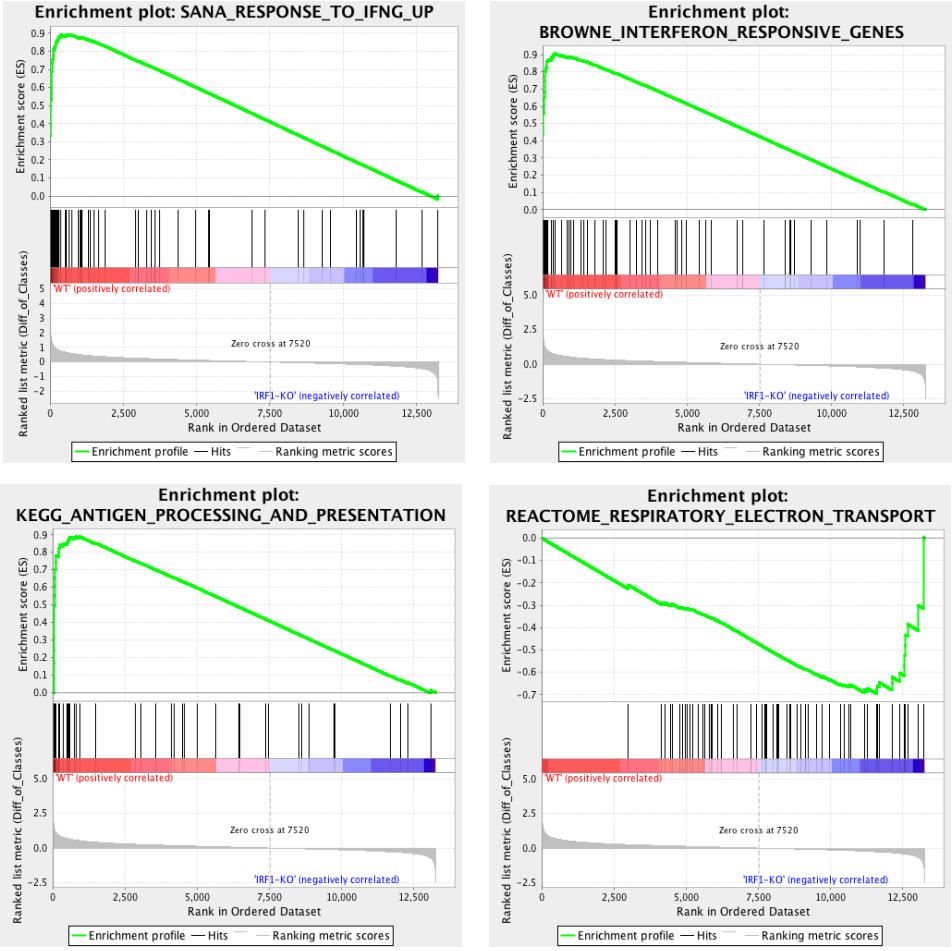

Figure 15: GSEA Enrichment plots for annotated signatures enriched either in IRF1-KO CFPAC1 or WT CFPAC1 cells in KO *vs* WT comparison.

The green plot shows the enrichment score of each annotated transcript in the gene set (black vertical bars), ranked left to right as per their enrichment in WT or KO cells. Top row: enrichment plots for Type I and Type II IFN related signatures (downregulated in IRF1-KO). Bottom row, left: antigen processing and presentation is downregulated in IRF1-KO cells. Bottom row, right: respiratory electron transport chain is upregulated in IRF1-KO cells.

V.7 ***IRF1 directly regulates the antigen processing and presentation pathway in PDAC cells***

To further analyse the main impact of IRF1 on the interferon related signatures, a type I/type II interferon signature was retrieved from the REACTOME database and its levels of expression in PDAC cell lines and the relative fold change of the same

transcripts in CFPAC1 WT vs IRF1- KO cells were compared (Fig. 16). As already highlighted from GO annotations, IRF1 deletion in low grade cells resulted in an overall downregulation of antigen processing and presentation-related transcripts, which in turn are the strongest differentially expressed genes in the signature in a low-grade *vs* high grade comparison. Among them, we found members of Class I MHC (*HLA-B*, *HLA-F*); of Class II MHC (*HLA-DMB*, *HLA-DQB1*, *HLA-DRB1*, *CD74*); of the immunoproteasome (*PSME1-2*, *PSMB8-9-10*); of the antigen processing machinery (*TAP2*, *PDIA3*, *ERP27*, *ERAP2*).

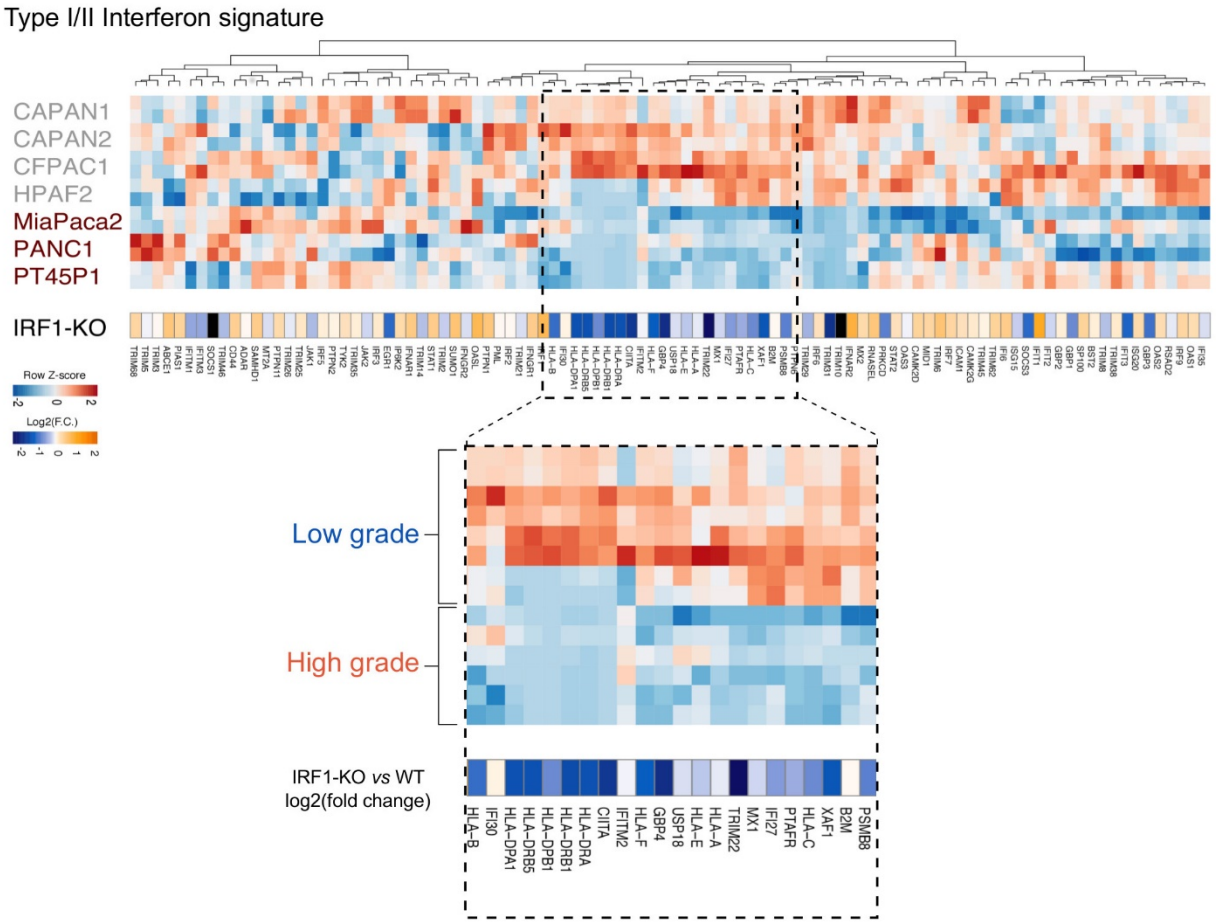

Figure 16: Downregulation of the interferon-related antigen processing and presentation pathway in IRF1-KO cells

Heatmap showing the expression levels of the interferon related signature retrieved from GO analysis on low grade vs high grade PDAC cells (top, values in TPM) and relative fold change upon IRF1 deletion in low grade cells (bottom label, $\log_2$(fold change)). Callout box highlights the downregulation of the antigen processing and presentation pathway.

To confirm this impaired expression of the antigen presenting molecules, a FACS analysis for both Class I and Class II MHC molecules was performed. As expected, a significant downregulation of both class I (HLA-ABC, p=0.0080, unpaired Student's T-test, two tailed); and class II molecules (pan-class II, p=0.0046, HLA-DP, p=0.0987, HLA-DQ, p=0.0026, HLA-DR, p=0.0079, unpaired Student's T-test, two tailed) was observed (Fig. 17).

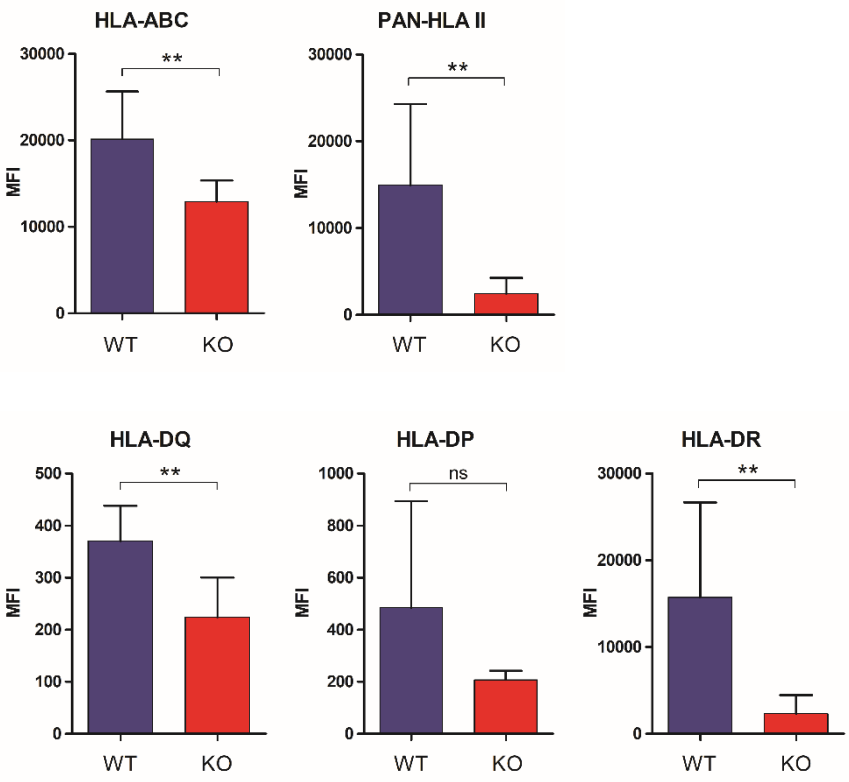

Figure 17: Expression of the antigen presenting molecules at the protein level upon IRF1 deletion.

FACS analysis (results shown as Mean Fluorescence Intensity) of HLAs in WT CFPAC1 cells and IRF1-KO cells. HLA-ABC, ** p=0.0080, pan-HLA II, **p=0.0046, HLA-DP, p=0.0987, HLA-DQ, **p=0.0026, HLA-DR, **p=0.0079, unpaired Student's T-test, two tailed.

To validate the contribution of IRF1 to the expression of members of this pathway in PDAC cell lines, this TF was ectopically expressed in both IRF1-KO CFPAC1 cells and in high grade PDAC cell lines (MiaPaca2, PANC1) (Fig. 18). The results showed that IRF1 overexpression was sufficient to rescue the antigen processing (PSMB8) and presentation (HLAs) pathway expression in IRF1-KO cells. Moreover, when overexpressed in high grade PDAC cell lines, a similar activation of the pathway was induced. These data together show that IRF1 is the main regulator of the antigen processing and presentation pathway in PDAC cells, and its absence impairs the expression of this pathway in high grade PDAC.

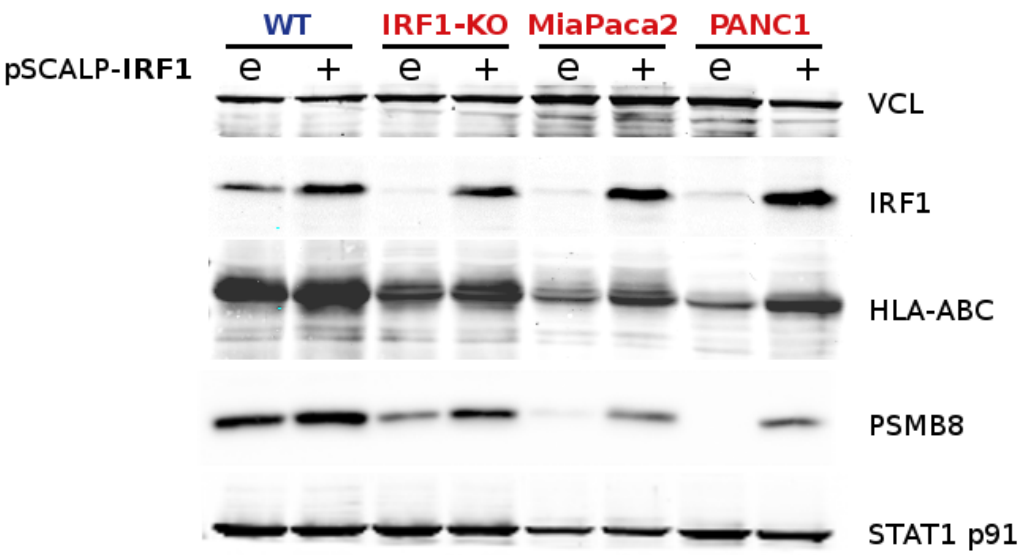

Figure 18: IRF1 overexpression in IRF1-KO CFPAC1 cells and in high grade PDAC cell lines

Western blot of PDAC cell lines infected with lentiviral expression vectors (pSCALP) either empty, as a control, (e), or containing IRF1 cds (+). Vinculin (VCL) is shown as a loading control.

V.8 *IRF1 is involved in the metabolic control of low grade PDAC*

As mentioned above (see Fig. 14), the transcriptional profiling of IRF1 deficient low-grade cells suggested a contribution of this TF to the control of metabolic networks in low grade PDACs. In particular, starting from GO analysis, it was of particular interest to investigate the impact it may have on the oxidative processes as well as onto the general metabolic landscape.

To investigate the involvement of IRF1 in the regulation of the oxidative phosphorylation processes, oxygraphic measurements were used to assess the mitochondrial activity. Oxygen consumption rate was measured in the basal state and in presence of specific chemicals to analyse the individual components of the respiratory chain. When the respiration rate, coupled and uncoupled to ATP synthesis, was assayed, a significant increase in the activity of the mitochondrial respiratory chain upon IRF1 deletion, at a basal level as well as when uncoupled from ATP synthesis could be observed. (Fig. 19. Basal respiration, p=0.0393; ADP-coupled respiration, p=0,0043; Oligomycin uncoupled respiration, p=0,0698; CCCP uncoupled respiration, p=0,0019, unpaired Student's T-test). Also, the activity of single complexes was measured (Complex I, Complex II, Complex IV), by the use of specific inhibitors and substrate combinations. Again, a substantial increase in the activity of the Complexes I and IV was observed (Fig. 20: Complex I, p=0,0276; Complex II, p=0,1194; Complex IV, p=0,0434, Unpaired Student's T-test) in IRF1-deficient cells compared to WT. These data were concordant with the observed increased expression of key members of the electron transport chain from the RNA-Seq experiment (e.g. *NQO1* NAD(P)H quinone dehydrogenase 1; *UQCRFS1* ubiquinol-cytochrome c reductase, 2C Rieske iron-sulfur polypeptide 1; *COX5A* cytochrome c oxidase subunit 5A). Overall, these data show an

augmented respiratory activity in low grade pancreatic cancer cells depleted of IRF1, compared to WT cells.

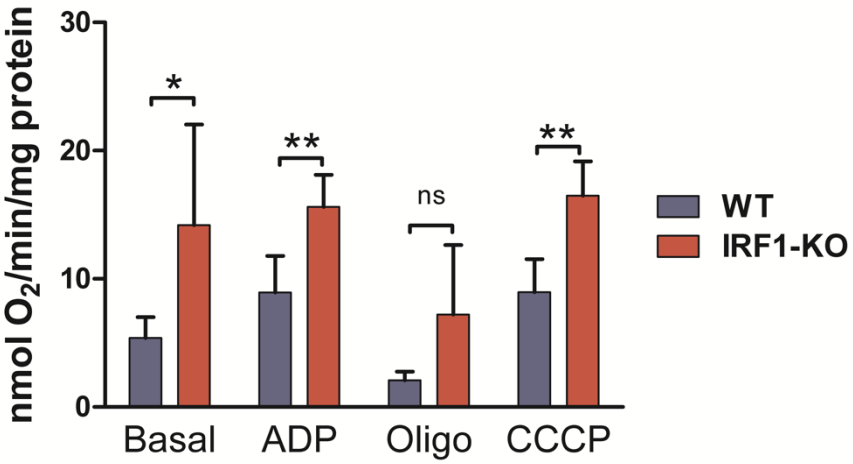

Figure 19: Respiration rates of IRF1-deficient and WT CFPAC1 cells

Histogram of oxygraphic measurements for WT (blue) and IRF1-KO (red) cells. Respiration rate is displayed as nanomoles of oxygen consumed per minute, normalized over protein content in mg. Basal respiration, *p=0.0393; ADP: ADP-coupled respiration, **p=0,0043; Oligo: Oligomycin uncoupled respiration, p=0,0698; CCCP: CCCP uncoupled respiration, ** p=0,0019. Unpaired Student's T-test.

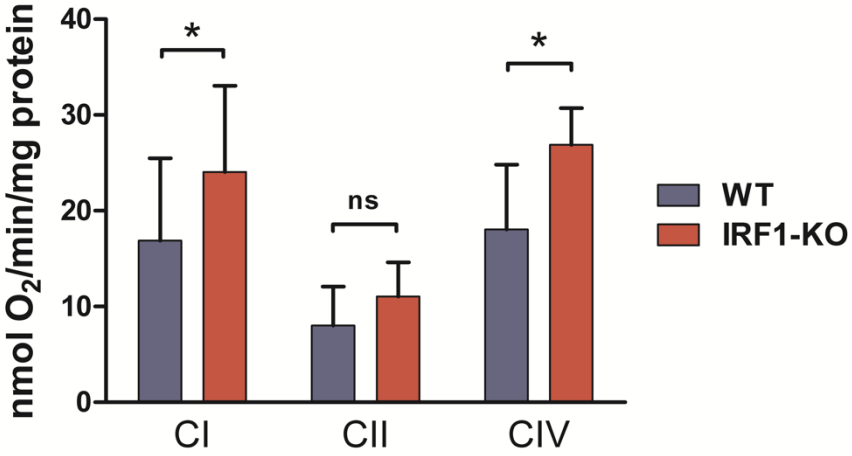

Figure 20: Activity of the complexes of the respiratory chain in IRF1-KO and WT CFPAC1 cells.

Histogram of oxygraphic measurements for WT (blue) and IRF1-KO (red) cells. Respiration rate is displayed as nanomoles of oxygen consumed per minute, normalized over protein content in mg. CI: Complex I activity, *p=0.0276; CII: Complex II activity, p=0,1194; CIV: Complex IV activity, *p=0,0434. Unpaired Student's T-test.

V.9 ***IRF1 deletion in low grade cells affects their metabolic profile, increasing lipogenesis***

RNA-Seq results displayed an enrichment in deregulated metabolic signatures in IRF1-KO cells. These changes were then investigated in a metabolome- and lipidome-wide study, using targeted LC-ESI-MS/MS against a library of standards encompassing all the main metabolic branches. From the overall metabolic profiling, a reduction in the levels of protein amino acids and an increase in hub metabolites of energetic metabolism could be observed in IRF1-KO cells. These metabolites included: Acetyl-CoA (needed for TCA cycle and lipogenesis, final product of glycolysis, β-oxidation, BCAA catabolism), Malonyl-CoA (lipogenesis intermediate), Fructose 1,6-bisphospate (key regulator of glycolysis) and ADP (Fig. 21). The lipidomic analysis showed a profound change in the lipid profile, with changes in the membrane lipid relative abundance and saturation levels. A reduction in the levels of cerebrosides of the sulfatides family was observed, as well as changes in the relative abundance of phosphatidylethanolamines (Fig. 22). In particular, long fatty acids-conjugated, poorly unsaturated, phosphatidylethanolamines were decreased, while species with shorter acyl chains and higher level of unsaturation were increased.

To gain a deeper understanding of the diverted metabolic networks resulting from IRF1 deletion, two different approaches were then used, the results of which were ultimately integrated in a metabolic model. First, data integration analysis of transcriptomics and metabolomics experiments using MetaboAnalyst [63] was performed. It was used to compare the list of deregulated transcript from the RNA-Seq experiment with the list of changing metabolites retrieved from the metabolomics study (IRF1-KO *vs* WT). A functional annotation of altered pathways was retrieved (see Fig. 23 a-b and Tab.1a-b). Affected pathways were ranked by the p-value of their

enrichment and by a topology (pathway impact) factor, which measured the relevance of the affected metabolites in a specific pathway. This annotation showed a negative effect on Glutamine and glutamate metabolism (although I could not be inferred whether it was in catabolism or anabolism), as well as in a number of pathways associated to glycerolipid, glycerophospholipid and glycosphingolipid metabolism (Fig. 23a, Tab. 1a). The positively impacted pathways retrieved a strong contribution in general carbon metabolism terms (TCA cycle, pyruvate metabolism, glycolysis) as well as in Pentose phosphate pathway and nucleobase metabolism (pyrimidine metabolism, purine metabolisms, amino sugar and nucleotide sugar metabolism) (Fig.23b, Tab. 1b).

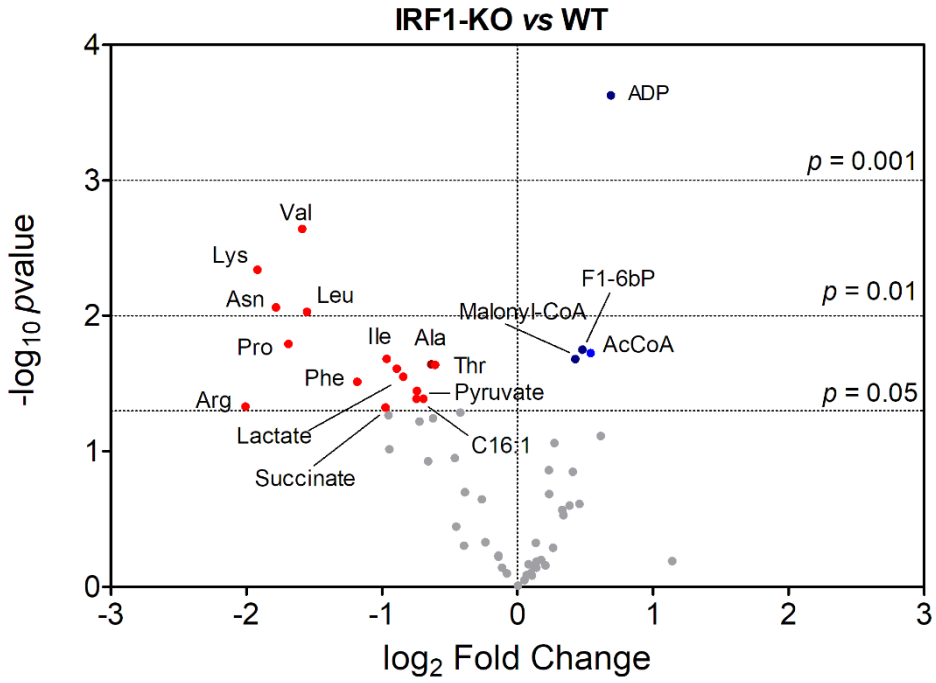

Figure 19: Effects of IRF1 deletion on the low grade PDAC cells metabolome.

Volcano plot depicting the affected metabolites in a IRF1-KO vs WT CFPAC1 cells comparison. Downregulated metabolites in IRF1-KO cells are highlighted in red. Upregulated metabolites in IRF1-KO cells are highlighted in blue.

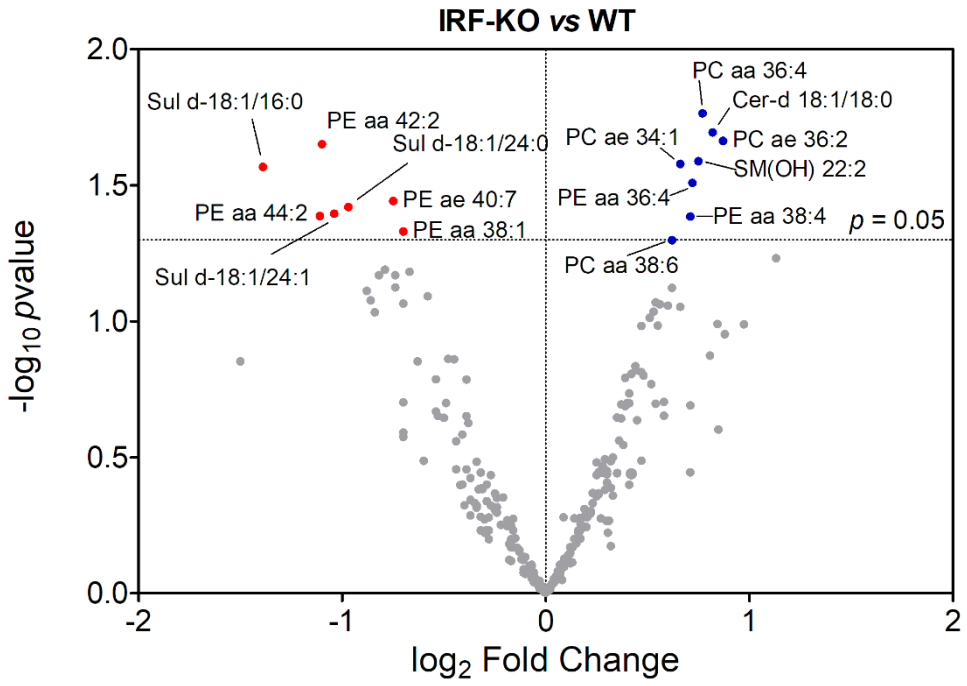

Figure 20: Effects of IRF1 deletion of low grade PDAC cells lipidome.

Volcano plot depicting the affected lipids in a IRF1-KO vs WT CFPAC1 cells comparison. Downregulated lipids in IRF1-KO cells are highlighted in red. Upregulated metabolites in IRF1-KO cells are highlighted in blue. PC: phosphatidylcholine; PE: phosphatidylethanolamine; Sul: sulfatide; SM: sphingomyelin. Aa: acyl-ester bond, ae: acyl-ether bond. Numbers (n:m): n: total acyl chains carbons. m: number of unsaturated bonds.

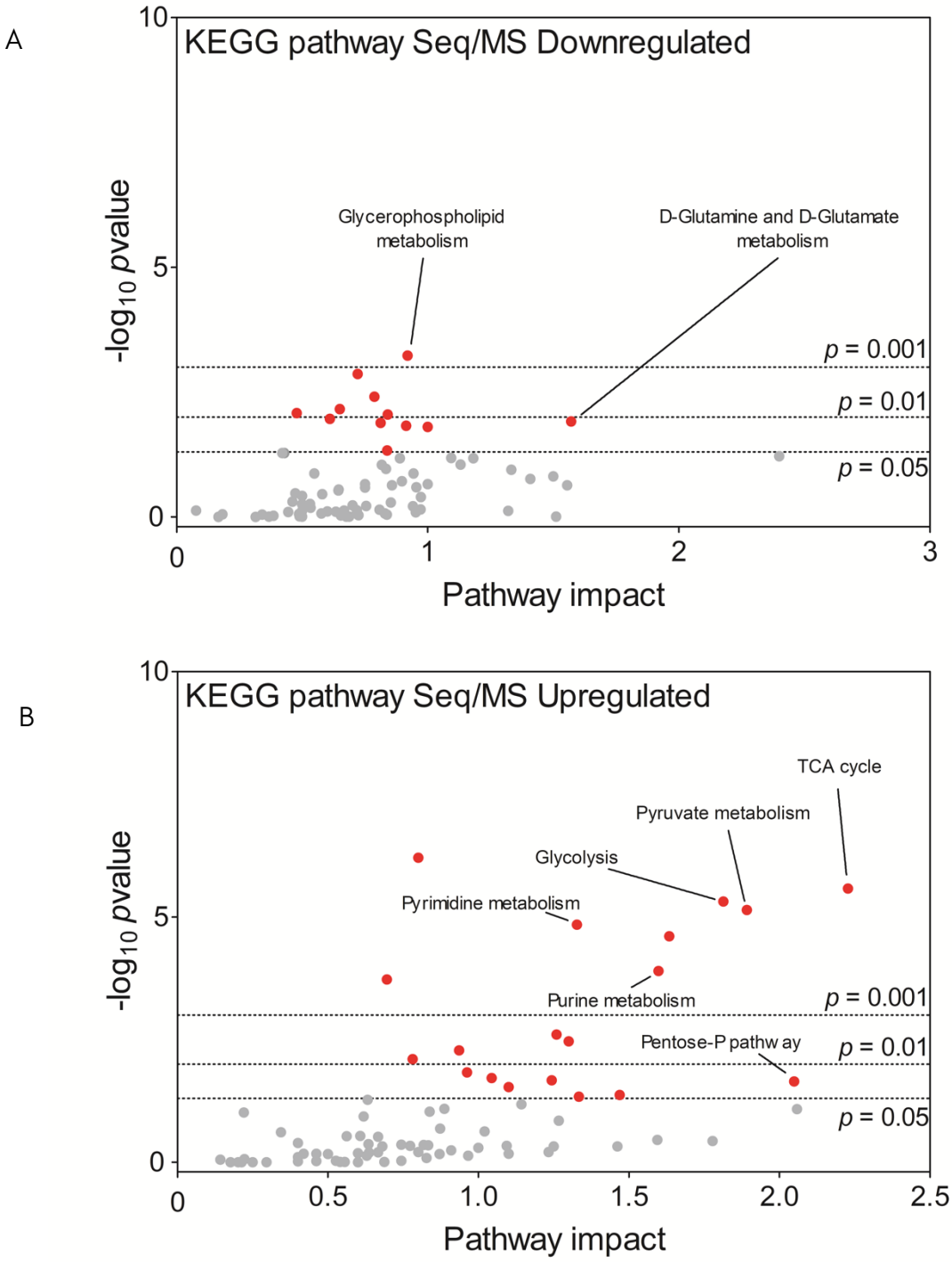

Figure 21: Data integration of RNA-Seq and Metabolomics experiments provide an overview of the affected metabolic pathways upon IRF1 deletion in low grade PDAC cells.

Scatter plots of pathways retrieved from a combined enrichment/topology analysis. Each dot represents a pathway from KEGG database. Significantly enriched pathways are highlighted in red (p-value ≤ 0.05, see Tab.1). (A): negatively enriched pathways in IRF1-KO vs WT comparison. (B) positively enriched pathways in IRF1-KO vs WT comparison.

A

Negatively impacted pathways		
Pathway name	Pathway impact	$-\log_{10}$ (p-value)
Glycerophospholipid metabolism	0,920	3,231
Lysine degradation	0,721	2,860
Purine metabolism	0,787	2,406
Mucin type O-Glycan biosynthesis	0,650	2,161
Aminoacyl-tRNA biosynthesis	0,478	2,079
Pyrimidine metabolism	0,841	2,052
Glycosphingolipid biosynthesis - lacto and neolacto series	0,610	1,961
D-Glutamine and D-glutamate metabolism	1,571	1,909
Inositol phosphate metabolism	0,813	1,883
Terpenoid backbone biosynthesis	0,914	1,823
Alanine, aspartate and glutamate metabolism	1,000	1,800
Glycerolipid metabolism	0,838	1,329

B

Positively impacted pathways		
Pathway name	Pathway impact	$-\log_{10}$ (p-value)
N-Glycan biosynthesis	0,800	6,205
TCA cycle	2,227	5,579
Glycolysis	1,814	5,317
Pyruvate metabolism	1,891	5,145
Pyrimidine metabolism	1,327	4,840
Propanoate metabolism	1,634	4,609
Purine metabolism	1,598	3,896
Aminoacyl-tRNA biosynthesis	0,696	3,723
Amino sugar and nucleotide sugar metabolism	1,259	2,603
Valine, leucine and isoleucine degradation	1,300	2,461
Glycosylphosphatidylinositol(GPI)-anchor biosynthesis	0,935	2,278
Inositol phosphate metabolism	0,781	2,101
Glutathione metabolism	0,962	1,832
Glycosphingolipid biosynthesis - ganglio series	1,044	1,713
Fructose and mannose metabolism	1,243	1,668
Pentose phosphate pathway	2,049	1,648
Glyoxylate and dicarboxylate metabolism	1,100	1,529
Galactose metabolism	1,469	1,372
Glycosphingolipid biosynthesis - globo series	1,333	1,338
Butirosin and neomycin biosynthesis	1,333	1,337

Table 1: Extended results from the pathway enrichment/topology analysis shown in Fig. 23.
Top: negatively enriched pathways in IRF1-KO vs WT comparison. Bottom: positively enriched pathways in IRF1-KO vs WT comparison.

A second approach to resolve the complexity of metabolic changes was to use carbon tracing metabolomics. Three different carbon sources fully labelled with a stable heavy carbon isotope, ^{13}C (with very rare natural occurrence) were used. Isotope distribution (as Mass Isotopomer Distribution, MID) was then measured in a targeted metabolomics experiment, so that it was possible to reconstruct the destiny of each carbon atom in the cell. These isotope distributions were then compared between WT and IRF1-KO CFPAC1 cells. The carbon sources used were: $^{13}C_6$-Glucose; $^{13}C_5$-Glutamine and $^{13}C_{16}$-Palmitate, each of them in a separate experiment. After treatment, several metabolites were measured by targeted LC-ESI-MS/MS. Fig. 24 shows all the measured metabolites and the main metabolic pathways which were investigated.

Labelled glucose tracing (Fig. 25) in IRF1- KO cells showed an overall increase in the activity of the pentose phosphate pathway, although there was no significant diversion of the glycolytic flux. Carbon flux in the TCA cycle is not affected, although changes in M2 isotopomers of Malate and Oxaloacetate suggest a diversion of the cycle through the activity of a Malic Enzyme. Ultimately, IRF1 deletion seems to increase the already strong lipogenic profile of these cells, with increased levels of carbon incorporation in fatty acid chains.

Glutamine usage (Fig. 26) in CFPAC1 cells seems to follow both the oxidative and the reductive pathways – although none of these pathways seems to be affected upon IRF1 deletion. The overall result again confirmed a high activity of malic enzyme 1 (ME1, NADP-dependent malate dehydrogenase, oxaloacetate decarboxylating) in IRF1-KO cells, as well as an increased lipogenic profile.

Labelled palmitate (Fig. 27) similarly provided evidence of increased activity, upon IRF1 deletion, of Malic Enzyme 1 – both as malate dehydrogenase as well as oxaloacetate decarboxylase– leading to pyruvate accumulation.

The resulting general model of the metabolic rewiring upon IRF1 deletion in low grade PDAC cells shows that IRF1 is able to regulate the lipogenesis in these cells (Fig. 28). Its deletion results in increased activation of the latter pathway. Concordantly, pathways and reactions resulting in the production of reduced NADPH are also upregulated (Pentose phosphate pathway, Malic Enzyme 1). This coenzyme, in fact, is needed for fatty acid synthesis as an electron donor. The observed changes serve to corroborate the impacted pathways highlighted in the enrichment/topology analysis. Pentose phosphate pathway upregulation upon IRF1 deletion was confirmed (which may also fit the "*purine metabolism*" and "*pyrimidine metabolism*" terms, highly enriched but with a lower pathway impact), as well as the impact, from the activity of Malic Enzyme 1, on "*TCA cycle*" and "*pyruvate metabolism*" terms.

These results, altogether, provided evidence that IRF1 is a regulator of the lipidic metabolism of low grade PDAC cells. In particular, this TF suppresses lipogenesis, as its deletion could hyperactivate this pathway (Fig.28). Moreover, it also controls glycerolipid synthesis (Fig. 23): in particular, it regulates the expression levels of *GPAT2* (downregulated in IRF1-KO cells), a key enzyme in this pathway. IRF1 deletion in low grade PDAC cells is also able to subvert the relative abundance and saturation levels of phospholipids and other membrane lipids (Fig. 22).

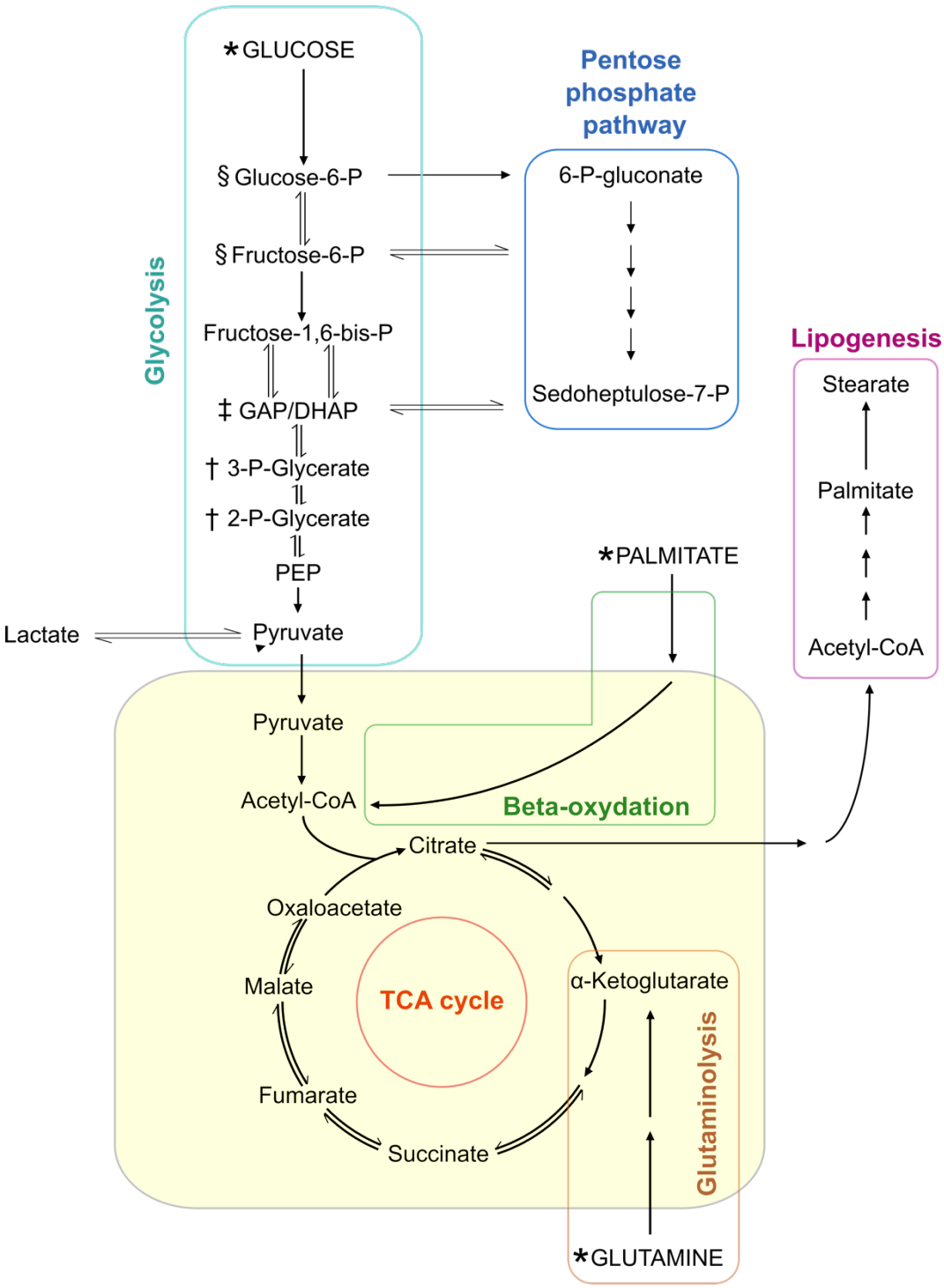

Figure 22: General model of the metabolic tracing experiment.

Metabolites provided as traced carbon sources are highlighted by asterisks. * Glucose-$^{13}C_6$; * Glutamine-$^{13}C_5$; * Palmitate-$^{13}C_{16}$. All the measured metabolites are shown. Orange box represents mitochondrion.

† 3-phospho-glycerate and 2-phosphoglycerate could not be spectroscopically resolved.

‡ Glyceraldehyde-phosphate (GAP) and Dihydroxyacetone-phosphate (DHAP) could not be spectroscopically resolved.

§ Glucose-6-phospate and Fructose-6-phosphate could not be spectroscopically resolved.

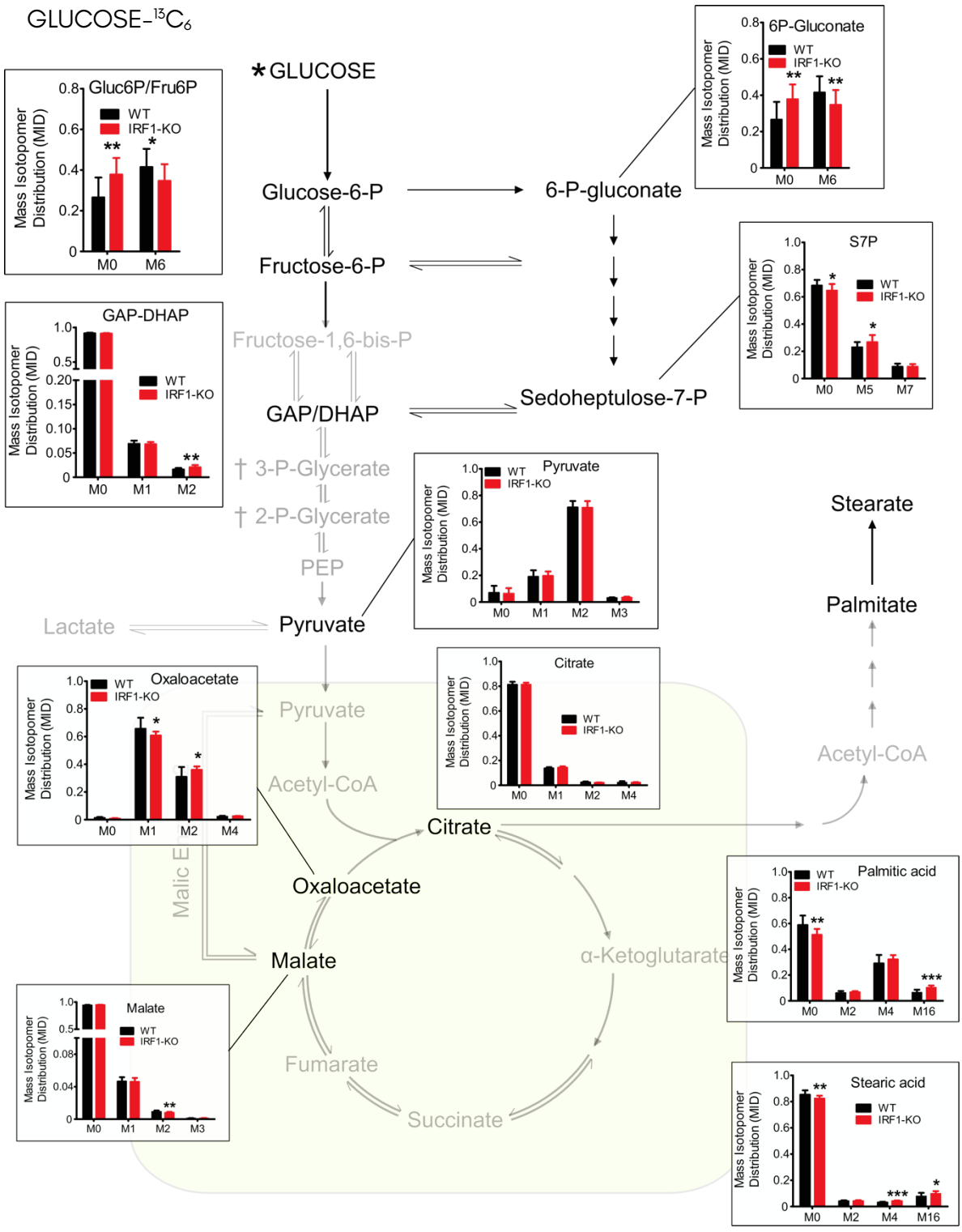

Figure 23: Carbon tracing experiment: labelled Glucose-$^{13}C_6$.

Callout boxes show the histograms of Mass Isotopomer Distribution (MDI) for the selected metabolites. Black bars WT CFPAC1 clones, Red bars: IRF1-KO clones. *: p-value ≤ 0.05; **: p-value ≤ 0.01; ***: p-value ≤ 0.001. Unpaired Students' T-test.

GLUTAMINE-$^{13}C_5$

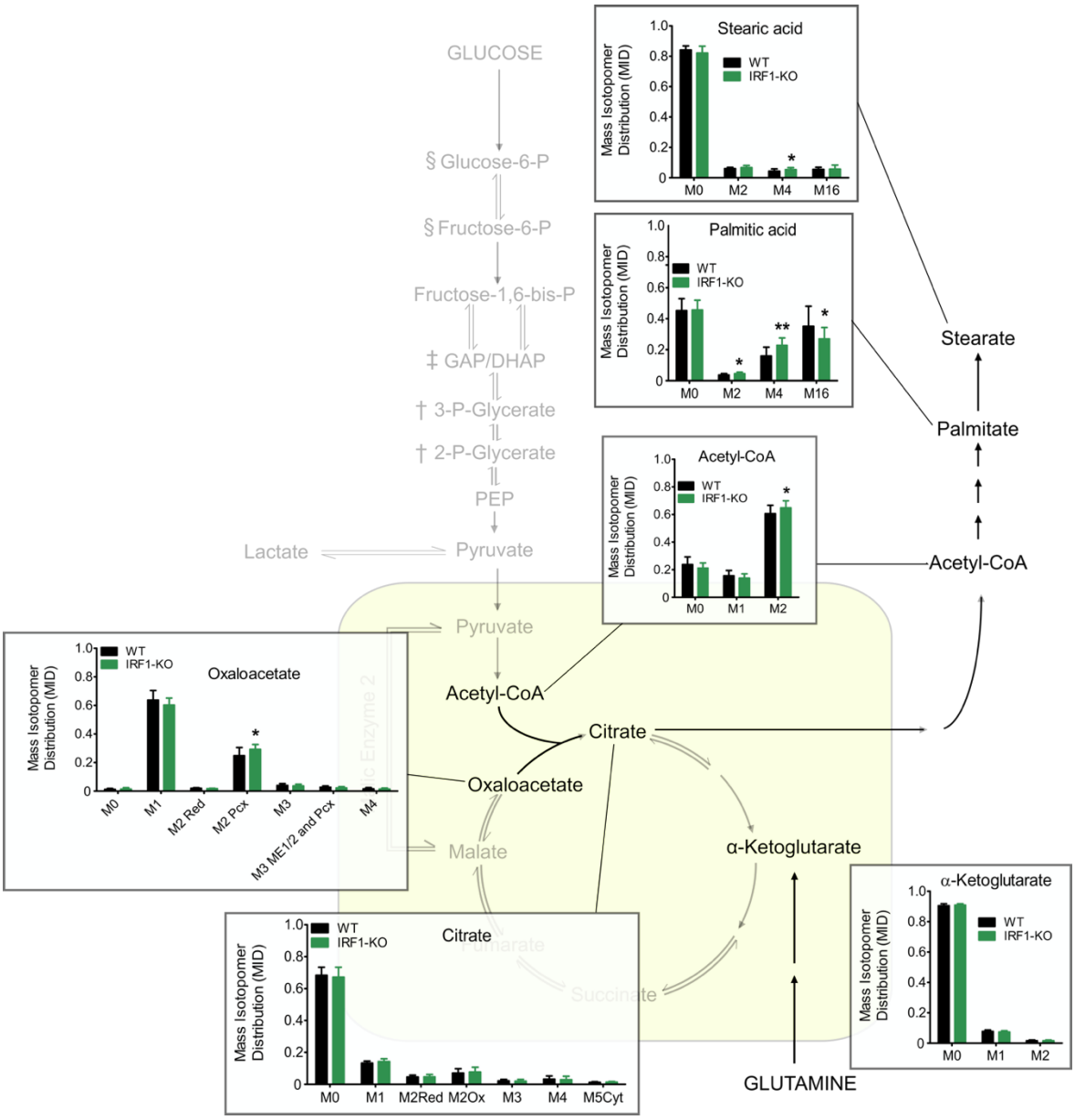

Figure 24: Carbon tracing experiment: labelled Glutamine-$^{13}C_5$.

Callout boxes show the histograms of Mass Isotopomer Distribution (MDI) for the selected metabolites. Black bars WT CFPAC1 clones, green bars: IRF1-KO clones. *: p-value ≤ 0.05; **: p-value ≤ 0.01; ***: p-value ≤ 0.001. Unpaired Students' T-test.

PALMITATE-$^{13}C_{16}$

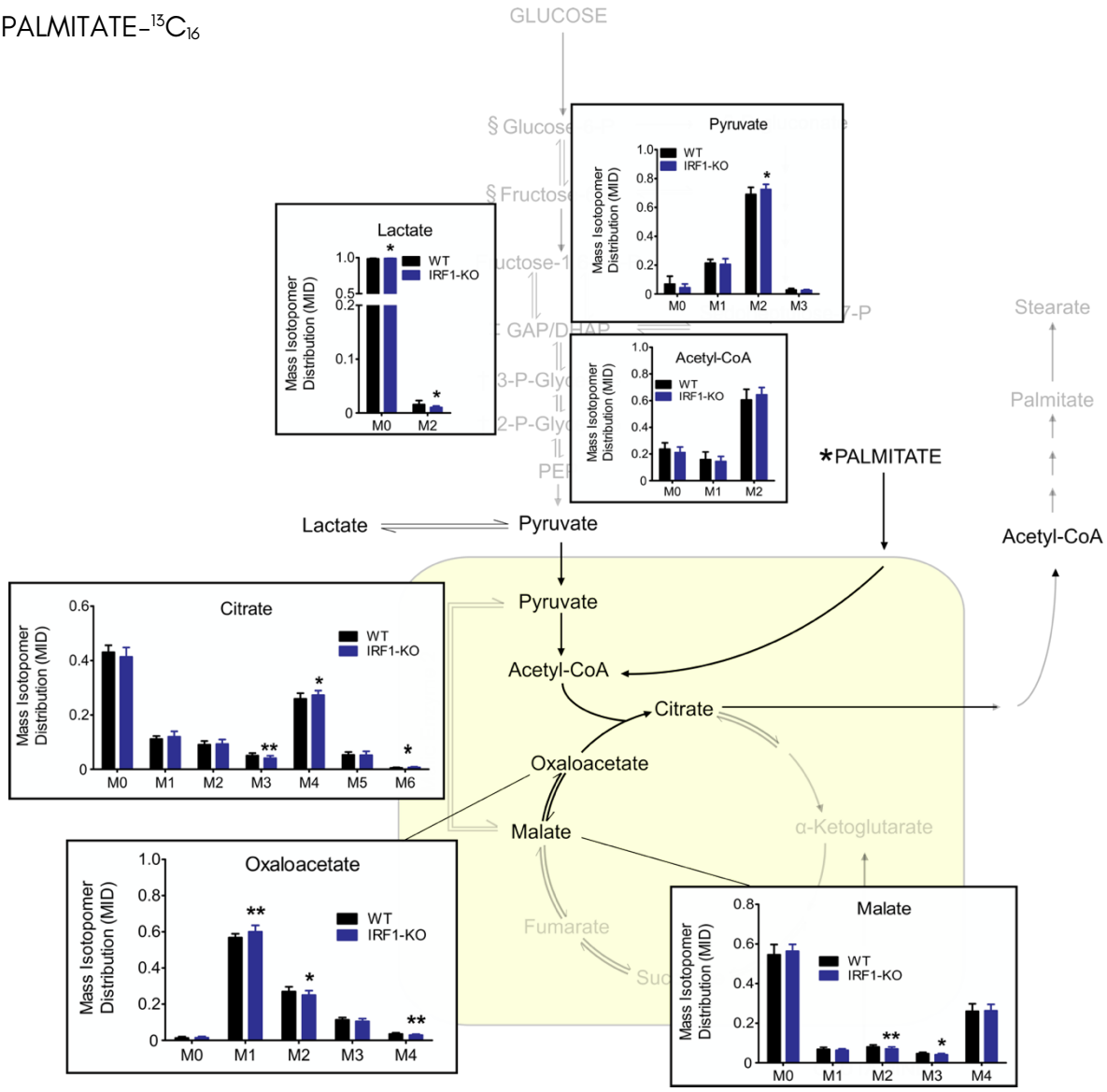

Figure 25: Carbon tracing experiment: labelled Palmitate-$^{13}C_{16}$.

Callout boxes show the histograms of Mass Isotopomer Distribution (MID) for the selected metabolites. Black bars WT CFPAC1 clones, blue bars: IRF1-KO clones. *: p-value ≤ 0.05; **: p-value ≤ 0.01; ***: p-value ≤ 0.001. Unpaired Students' T-test.

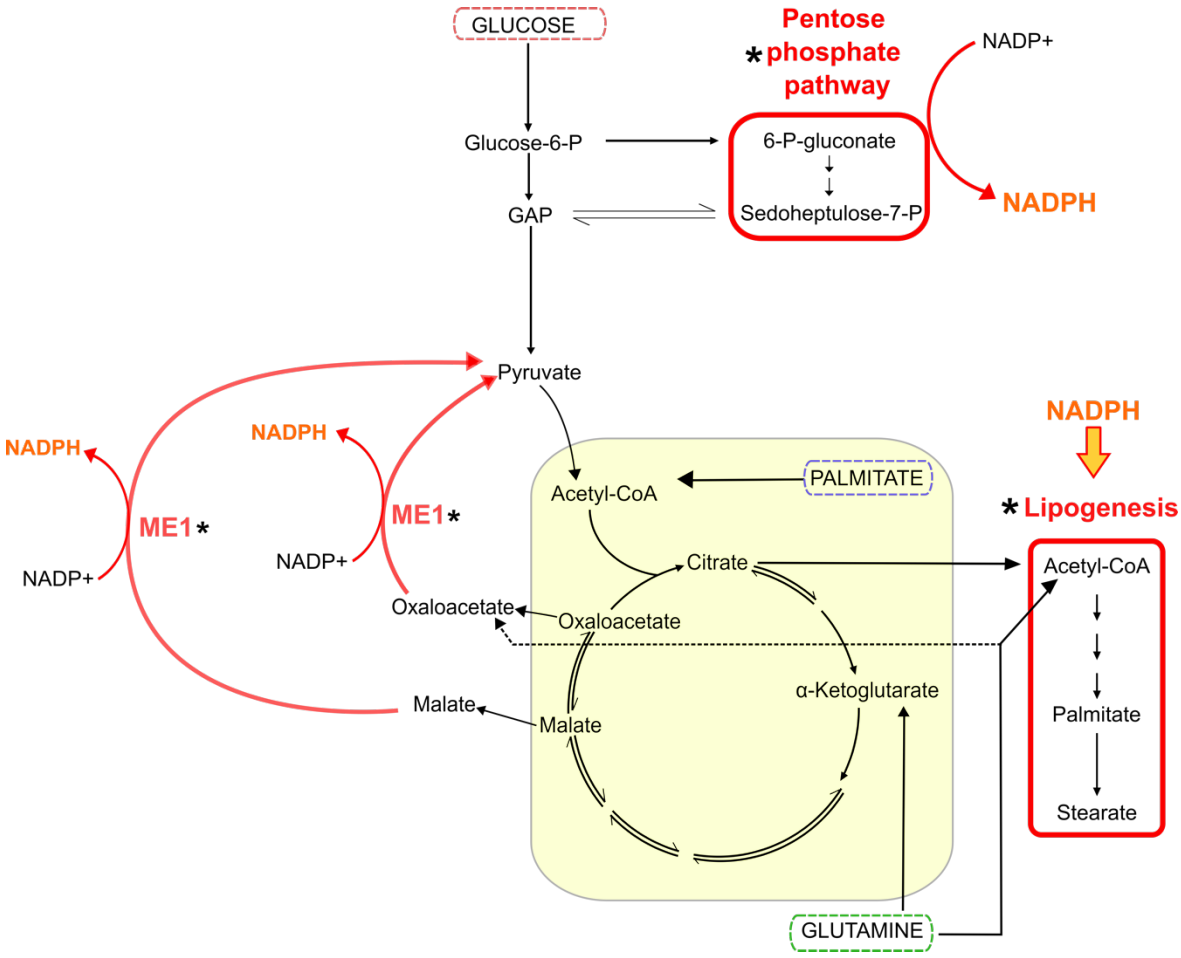

Figure 26: Proposed model of the metabolic rewiring upon IRF1 deletion in low grade PDAC cells.

Metabolites provided and traced as carbon sources are highlighted by dotted boxes. Orange box represents mitochondrion. Asterisks and red boxes and lines highlight the hyperactivated pathways and reactions after IRF1 deletion: *Lipogenesis; *Pentose Phosphate Pathway; *Malic Enzyme 1. NADPH production by Pentose phosphate pathway and ME1 activity is used as reductive substrate in fatty acid synthesis.

VI. Materials and Methods

VI.1 Cell lines and culture conditions:

The following human PDAC cell lines were used: CFPAC-1 (ATCC CRL-1918), CAPAN-1 (ATCC HTB-79), CAPAN-2 (ATCC HTB-80), MiaPaCa-2 (ATCC CRL-1420), PANC-1 (ATCC CRL-1469), PT45P1 (obtained from Paola Allavena, Humanitas Research Hospital, Rozzano), HPDE6 (obtained from Paola Allavena, Humanitas Research Hospital, Rozzano), HEK293T (ATCC CRL-3216). Cells were maintained in IMDM+10% FBS (CFPAC-1); RPMI+10% FBS (PT45P1); RPMI+15% FBS (CAPAN-2); RPMI+20% FBS (CAPAN-1); DMEM+10% FBS (MiaPaCa-2, PANC-1, HEK293T); KSF + [0.05 mg/ml] Bovine Pituitary Extract + [5 ng/ml] EGF (HPDE6). Media were all supplemented with 2 mM L-glutamine.

VI.2 Antibodies and reagents:

For Western blots the following primary antibodies were used: STAT1 (CST, 9172); p-STAT1-Y701 (CST, 7649); IRF1 (CST, D5E4); HLA-ABC (Abcam, ab70328); PSMB8 (Abcam, ab3329), STAT1 p91 (Santa Cruz, sc-345), TUBULIN (Santa Cruz Biotechnology, sc-8035); VINCULIN (Sigma-Aldrich, V9131). For immunohistochemistry the following primary antibodies were used: IRF1 (Abcam, ab191032), IBA1 (Wako, 019-19741). Envision anti-rabbit-HRP polymer (Dako) was used as secondary antibody.

Human interferon beta 1a for cell line treatment was purchased from PBL assay science (11415-1, Lot N°6174). Cell were plated in 6 well plates and treated 2 hours at 100 U/ml in their own medium, then collected for RNA and protein extraction.

VI.3 ***SDS-PAGE:***

Cells were lysed in RIPA buffer containing protease inhibitors, and 50 μg of clarified cell extracts were resolved on SDS-polyacrylamide gel, blotted onto nitrocellulose membranes. After blocking in 5% milk in TRIS Buffer Saline, 0,1% Tween, membranes were probed with the antibodies o.n. at 4°C, washed and probed with the respective secondary antibodies, HRP conjugated. Chemiluminescent signal was revealed using Clarity ECL (Biorad).

VI.4 ***Quantitative PCR:***

RNAs were extracted using the Maxwell total RNA extraction kit (Promega) and 1 ug was retrotranscribed to cDNA using ImProm-II reverse trascriptase kit (Promega). Quantitative PCR reaction was assembled using Fast SYBR green master mix (Applied Biosystems). The following primers were used. C1ORF43 was used as reference gene based on the analysis of data from the Human BodyMap (HBM) 2.0 Project.

CAACATGCCCATCACTCGGA	IRF1_fw
TGCTTTGTATCGGCCTGTGT	IRF1_rev
CACCGTGACGGATATGGTCC	MX1_fw
GCACCCCTGTATACCTGGTC	MX1_rev
ACATTGACAGAGCCTGGACG	GBP2_fw
GGGTGTTGTTCCCCAGATCA	GBP2_rev
GGATGAAAGCTCTGGATGCC	C1ORF43_fw
GCTTTGCGTACACCCTTGAA	C1ORF43_rev

VI.5 ***Immunohistochemistry and histochemistry:***

Tumour microarray (TMA) of PDAC patients (PA1002a) was purchased from US Biomax. For immunohistochemistry, FFPE slides were deparaffinised in xylene, rehydrated using decreasing alcohol progression, then subjected to heat induced epitope retrieval using citrate buffer (10mM Sodium Citrate, 0.05% Tween 20, pH 6.0) for 15' using a microwave oven. After blocking, samples were incubated with the specific primary antibody (4°C, 4 hours for IRF1, 4°C, o.n. for IBA1), washed three times with 0,05% BSA in Dulbecco Phosphate Saline Buffer, incubated for 1 hour at room temperature with the secondary antibody and washed. Signal was revealed using DAB (Dako). Counterstaining was performed using Mayer's haematoxylin (Sigma). Images were acquired using Olympus-BX63 upright microscope or Olympus upright BX51 microscope linked to a Nikon DS-5Mc colour camera.

Histochemical staining of collagen fibres was performed using Picrosirius Red stain kit (Polysciences Inc.) and counterstained with Weigert's Haematoxylin Kit (Polysciences Inc.). Briefly, FFPE slides were deparaffinised in xylene and rehydrated using decreasing alcohol progression, then counterstained with Weigert's Haematoxylin for 2 hours. Then treated for 2' with Phosphomolybdic acid, rinsed, 1 hour with Picrosirius Red, 2' with 0.01 N HCl, dehydrated and mounted. Images were acquired using Olympus-BX63 upright microscope equipped with a polarized filter.

VI.6 ***Image analysis and quantification:***

For TMA quantification of IRF1 positive tumour cells the open-source QuPath software was used (https://qupath.github.io/) [64]. Briefly, TMA images were imported as RGB files and TMA dearraying, colour deconvolution, cell segmentation using haematoxylin were performed. User-instructed sampling of tumour/non-tumour

areas was used to build a random forest classifier to be applied across all TMA cores. Manual definition of ROIs was used to subsample the spots according to local histological grade (G1 to G3). For each ROI, IRF1 positive tumour cells over total tumour cells were quantified.

For IBA1 immunohistochemistry, manual counting of IBA1 positive cells was performed. For Picrosirius Red, 20x magnification fields were used, 2 fields per condition (5 WT vs 5 KO). RGB Images were imported to FIJI (https://fiji.sc/), green and red channels were extracted and background was subtracted. Resulting channels were binarised and mean grey values were measured.

VI.7 ***CRISPR-Cas9 mediated genome editing:***

The sgRNA 5'-CTCATGCGCATCCGAGTGAT-3' targeting Exon 2 in the IRF1 gene was designed using http://crispr.mit.edu/ design platform. Its sequence was cloned into LentiCRISPR v2 vector (Addgene #52961 [65]) with EcoRI-XbaI extremities. Vector sequence was verified by Sanger sequencing. Lentiviral particles were produced using Calcium phosphate transfection of HEK293T cells with lentiCRISPRv2-sgIRF1 (or empty vector) and packaging vectors pMD2.G (Addgene #12259) and psPAX2 (Addgene #12260). To obtain IRF1-KO CFPAC1 clones, CFPAC1 cells were plated to subconfluency and transducted twice with the lentiviral particles carrying lentiCRISPRv2-sgIRF1 or the empty vector. Cells were selected by puromycin and serially diluted to obtain individual clones. Successful deletion was assessed using Surveyor assay [66] with the following primers:

AGAAGGGAAGAAGGCAGGAG	IRFSUR1
CTGGAGGGAATCGTGACCTA	IRFSUR2

The deletion in selected clones was confirmed by Western blot and Sanger sequencing.

VI.8 ***Interferon locus PCR:***

Genomic DNAs from cell lines were lysed using guanidine hydrochloride lysis and extracted using SeraMag beads (Sigma). 100 ng of gDNA per reaction were used. PCR reaction were carried out using Taq polymerase (NEB, M0273). 2.5% TAE-Agarose gel was used to resolve bands. Size was assessed using PCR ladder (NEB, N3234). GAPDH promoter primers were used as a positive control (Upstate, # 22-004). The following primers were used.

TCCTCAGAAGTCTTTGAGTCCTC	IFNE_FW
AGGAATTTCTCCGTGTGGTTTTC	IFNE_REV
ATGACCAACAAGTGTCTCCTCC	IFNB_FW
TTCAATTGCCACAGGAGCTTC	IFNB_REV
CAGTCAGCATGGTCCTCTGTA	IFNA2_REV
TCCAAAAGGCTGAAACCATCC	IFNA2_FW
CTACACAGCCCAACCAAACC	UPSTR_FW
TGTCTTTGGCAAATCAGGGC	UPSTR_REV
TTCGGCCAGCTTTGGATTATG	DNSTR_FW
TCCAGAAAGAGAGAATGGGCA	DNSTR_REV

VI.9 ***Adhesion assay:***

To measure matrix specific adhesion, coverslips were coated for 2 hours at 37°C with matrix solutions. After 1 hour of blocking with 5%BSA in DPBS, 10.000 cells per coverslip were plated (2 replicates, 3WT vs 3 IRF1-KO clones). After 1 hour at 37°C, coverslips were washed with DPBS and fixed with 4%PFA, 20', R.T.. Fixed cell were stained with toluidine blue (1% in water) for 20' at R.T., then excess stain was washed.

10X magnification pictures of each coverslip were taken. Cell counts were made using FIJI (https://fiji.sc/): "Remove background"> "Adjust Threshold"> "Make Binary" > "Analyze particles". The following matrices were used:

Matrix	Ref.	Concentration
Collagen	Sigma #C3867	20 µg/ml
Laminin	Roche #11243217001	10 µg/ml
Fibronectin	Roche #1180938001	10 µg/ml
Matrigel	BD #356231	20 µg/ml
Poly-D-Lys	Sigma #P6407	10 µg/ml
BSA		5%

VI.10 ***Circularity index:***

Circularity index measurements were performed using FIJI (https://fiji.sc/). Briefly, 7 WT and 7 IRF1-KO CFPAC1 clones were plated into 6-well plates, 200.000 cells/well. 24 hours after plating, 10x magnification pictures of at least two different fields per well were taken. 25 cells per clone were selected and outlined by hand. Circularity index (circularity=4π(area/perimeter^2)) was measured.

VI.11 ***Random migration:***

Random migration assay was performed as follows. 3 WT and 3 IRF1-KO clones were plated in 12-well plates, 50.000 cells per well, in duplicate. 24 hours later, live imaging of 5 separate fields per well was started, for 24 hours with a 5' period. An Olympus IX81 microscope equipped with an incubation chamber was used (37°C, 5% CO_2). Time-lapse movies were analysed using FIJI plugins "Manual tracking" to track 25 cells

per clone (75 cells per condition). Cumulative migration plots and relative analysis were performed using FIJI plugin "Chemotaxis Tool".

VI.12 ***Xenotransplants:***

Mouse xenografts were generated and collected in accordance with the Italian laws (D.L.vo 116/92 and following additions), which enforce the EU 86/609 directive, and under the control of the institutional organism for the animal welfare (Cogentech OPBA). Nude mice (n = 5 for each group) were injected with 5 million cells (CFPAC-1 WT clones, CFPAC-1 IRF1-KO clones) resuspended in 400 µl of DPBS under the skin of their hind flank. Subcutaneously injected mice were harvested 21 days after injection, fixed in 4% paraformaldehyde, and processed for paraffin embedding. Tumour mass measurements were taken every 3-4 days using a caliper to measure the two maximal diameters of the masses.

VI.13 ***FACS measurement of HLA expression:***

For FACS analysis of HLAs expression, 7 WT and 7 IRF1-KO CFPAC1 clones were analysed. Cells were detached using Versene (Lonza, #17-711E), resuspended in DPBS. HLA expression was assayed using the following antibodies: HLA-ABC (eBioscience, clone W6/32), HLA-DR (clone HB55), HLA-DP (clone B7/21), HLA-DQ (clone SPVL3), pan-HLAII (clone HB-145) using a LSRFORTESSA (BD) cell analyser. Human monocytes from blood were used as a positive control.

VI.14 ***IRF1 overexpression:***

IRF1 was cloned into the lentiviral construct pScalps-hygro-IRF1 (derivative of pScalps_puro, Addgene #99636) using BamHI-NotI extremities. Lentiviral particles were produced as described above and used to transduce cells (including empty

controls). 24 hours after infection, cells were selected for hygromycin resistance and harvested 48 hours later for downstream analysis.

VI.15 ***Heatmap of available expression data:***

Expression data from the type I/type II IFN signature in Diaferia *et al.* [3] were clustered according to their FPKM values. The minimum FPKM value was forced to 0.1 and subjected to log2-transformation. The distribution of values for each gene was then converted to z-scores. Heatmaps were designed using R.

VI.16 ***RNA-Seq of IRF1-KO vs WT cells, sample preparation and sequencing:***

RNA from 4 WT and 3 IRF1-KO CFPAC1 clones were extracted using Maxwell total RNA extraction kit (Promega). Libraries of cDNA for next generation sequencing were prepared using the SMART Seq2 protocol as in Picelli *et al.* [67] with minor modifications. Briefly, after reverse transcription of 5 ng of RNA using Superscript II reverse transcriptase (Thermo Scientific, #18064014), oligo-dT and a template switch oligo for second strand amplification, resulting cDNA was preamplified using KAPA HiFi HotStart DNA Polymerase (Roche, #07958897001) and purified. cDNA was purified and tagmentated using homemade Tn5 enzyme [68]. Lastly, tagmented cDNA was amplified using indexed primers for next generation sequencing to obtain a library. Samples were sequenced using an Illumina HiSeq 2000 platform.

VI.17 ***RNA-Seq analysis and differentially expressed genes calling:***

After quality filtering according to the Illumina pipeline, 50 bp single-end reads were aligned to the GRCh38/hg38 human reference genome and to the Homo sapiens

transcriptome (NCBI RefSeq) using TopHat2 (version 2.1.0) [69] with the option "--b2-very-sensitive". Only uniquely mapped reads were retained. At the gene level, expression counts were estimated using featureCounts (Rsubread version 1.5.1 [70], summarized across all exons as annotated in NCBI RefSeq hg38, with option "--largestOverlap". Both coding and long noncoding genes were retained for downstream analyses. Differentially expressed genes in four wild type and three IRF1-KO CFPAC1 clones were identified using EdgeR R-package (version 3.2.2) [71]. Prior to normalization using the Trimmed Mean of M (TMM) method, only genes with more than 1 CPM (Count Per Million) in at least three of the samples were retained. A common dispersion was estimated for all genes to measure the global biological variation (with option robust ="TRUE"). A negative binomial generalized log-linear model was fitted to each gene, and likelihood ratio tests were performed to assess differential expression. Genes were identified as differentially expressed when the following criteria were met: absolute log2 fold-changes (FC) $\geq$ 0.7, false discovery rate (FDR) < 0.05 and also had at least 1 TPM in at least 3 samples for conditions.

VI.18 ***Gene Ontology analysis and Gene Set Enrichment analysis:***

Gene Ontology (GO) enrichment analysis were performed using DAVID tools [61] in which deregulated gene list were used as target set and as a background set a complete list of expressed genes. REVIGo [72] was used to summarize the resulting significant GO terms and reduce redundancy. Gene Set Enrichment Analysis (GSEA) [62] was performed using all expressed genes ranked by the difference of classes and 1,000 gene set permutations. Gene sets background was building using the curated

gene sets collection c2.all.v5.2.symbols.gmt downloaded from the Molecular Signatures Database (MSigDB).

VI.19 ***Oxygraphic measurements of respiratory acitivity:***

Oxygraphic measurements were performed as described in Audano *et al.* [73]. All measurements were performed using a Clark type oxygen electrode (Hansatech, DW1 electrode chamber).

For coupled respiration measurements, detached WT and IRF1-KO CFPAC1 cells were rinsed in pre-warmed PBS (37°C) and suspended in coupled respiration buffer (2% free fatty acids-BSA, 1 mM Na-pyruvate, 25 mM D-glucose, 40 µg/ml digitonin). Samples were then transferred to the electrode chamber for the oxygen consumption rate measurement. After measuring basal respiration, uncoupled and maximal respiration were evaluated by adding 10 µM oligomycin and 10 µM CCCP, respectively. All samples values were normalized on total protein content.

Complex I, II, and IV activities were also assessed. Cells were resuspended in electron flow buffer (2% free fatty acids-BSA, 10 mM Na-pyruvate, 2 mM malate, 4 µM carbonyl cyanide m-chlorophenyl hydrazine (CCCP), digitonin 40 µg/ml). After cell transfer into the chamber, CI activity was evaluated. After 10 µM rotenone and 5 mM succinate addition, we assessed complex II activity. We then added 100 µM antimycin A and 20 mM/0.8 mM ascorbate/N,N,N',N'-tetramethyl-p-phenylenediamine (TMPD) to measure complex IV activity. All samples values were normalized on total protein content.

VI.20 ***LC-ESI-MS/MS analysis of metabolites and lipids and carbon flux analysis:***

For mass spectrometric investigation of metabolites and lipids, WT and IRF1-KO CFPAC clones (3 WT vs 3 IRF1-KO, 2 technical replicates per clone) were grown in 6-well plates and harvested in ice-cold PBS. Pellets were then resuspended in 250µl methanol/acetonitrile 1:1 containing [U-$^{13}C_6$]-Glucose- 1ng/µl (internal standard, Sigma Aldrich, 389374) and spun at 20,000g for 5 min at 4°C. Supernatant were then passed through a regenerated cellulose filter, dried and resuspended in 100µl of MeOH for subsequent analysis. Amino acids quantification was performed through previous derivatization. Briefly, 50µl of 5% phenyl isothiocyanate (PITC) in 31.5% EtOH and 31.5% pyridine in water were added to 10µl of each sample. Mixtures were then incubated with PITC solution for 20 min at RT, dried under N_2 flow and suspended in 100µl of 5mM ammonium acetate in MeOH/H2O 1:1. After centrifuging for 3 min at 20,000g at 4°C, samples were dried under nitrogen flux, resuspended in 200µl of MeOH and passed through a regenerated cellulose filter. Then, samples were dried again and resuspended in 100µl of MeOH for subsequent analyses. Metabolomic data were performed on an API-4000 triple quadrupole mass spectrometer (AB Sciex) coupled with a HPLC system (Agilent) and CTC PAL HTS autosampler (PAL System). The identity of all metabolites was confirmed using pure standards. Quantification of different metabolites was performed with a liquid chromatography/tandem mass spectrometry (LC-MS/MS) method using a C_{18} column (Biocrates) for amino acids and cyano-phase LUNA column (50mm x 4.6mm, 5 m; Phenomenex). Methanolic samples were analyzed by a 10 min run in positive (amino acids) and 5 min run in negative (all other metabolites) ion mode with a 20 multiple reaction monitoring (MRM) transition in positive ion mode and 30 MRM transition in negative ion mode, respectively. The mobile

phases for positive ion mode analysis (amino acids) were phase A: 0.2% formic acid in water and phase B: 0.2% formic acid in acetonitrile. The gradient was T0 100%A, T5.5min. 5%A, T7min 100%A with a flow rate of 500 l/min. The mobile phase for negative ion mode analysis (all other metabolites) was phase A: 5 mM ammonium acetate pH 7.00 in MeOH. The gradient was 100%A for all the analysis with a flow rate of 500 l/min. MultiQuant™ software (version 3.0.2) was used for data analysis and peak review of chromatograms. Quantitative evaluation of all metabolites was performed based on calibration curves with pure standards, then data were normalized on micrograms of protein.

For metabolic tracing analyses, WT and IRF1-KO CFPAC1 clones (3 WT vs 3 IRF1-KO, 5 technical replicates per clone) were exposed for 12 hr to [U-$^{13}C_6$]-Glucose 1mM (Sigma Aldrich, 389374) or [U-$^{13}C_5$]-Glutamine 2mM (Sigma Aldrich, 605166) or [U-$^{13}C_{16}$]-Palmitate 100µM (Sigma Aldrich, 605573). Metabolites quantification was performed as described above by increasing the MRM transitions in negative ion mode to 139 to analyze the different isotopomers.

VI.21 ***Pathway impact topological analysis:***

Pathway topological analysis was performed using MetaboAnalyst platform (http://www.metaboanalyst.ca) [63]. Lists of differentially expressed transcripts and differentially abundant metabolites and their relative fold changes were provided as inputs to retrieve a joint RNA-metabolite pathway integration.

VI.22 ***Statistical analysis:***

All statistical analysis present in the results section were performed using the indicated tests, using GraphPad Prism v.7.

VII. Discussion

This thesis aims to elucidate the link between the epithelial phenotype of low grade PDACs and the expression of an interferon-related signature. Here, I hypothesised that this signature, as observed in a previous differential expression analysis in a low grade PDAC vs high grade PDAC cell line model [3], was attributable to a grade-specific transcriptional dependency. The data in this work provide evidence that the TF IRF1, differentially expressed between PDACs of different grade, is responsible for the maintenance of the low grade-specific interferon signature. Low grade PDAC cells, in fact, when deprived of IRF1, downregulate the interferon-related pathway, and most notably, antigen processing and presentation. Moreover, it was shown here that IRF1 is a metabolic regulator in PDAC cell lines, mainly regulating the lipidic profile and related metabolism.

VII.1 ***The interferon signature of low grade PDAC cells is linked to a cancer-cell autonomous transcriptional network***

One could argue that the activation of the interferon-signature was related to a differential autocrine production of interferons in our cell line model. As such, I assessed the mutational status of the type I IFN locus. This genomic region, containing all the type I IFN genes, is located roughly 0.5 Mbp downstream of the *CDKN2A* locus, and the co-deletion event is a frequent feature of PDAC cell lines [60, 74]. Moreover, in melanoma, it has been shown that copy number variations of the type I IFN genes affect the expression of a general interferon signature, and consequently the response to MEK inhibitors [50]. However, I found no association between cell line grade,

signature expression and type I IFN locus integrity. It is possible, therefore, to rule out a link between IFN locus deletion and the interferon signature of PDAC cells of different grade. Nonetheless, the heterogeneous mutational status of this locus should be addressed in the future as a possible player in clonal selection of PDAC. Although type I IFNs have always been described as the classical non-immune IFNs [22], further investigations on different cytokine signalling pathways may serve to provide additional insight into the mechanism of action.

I also considered the hypothesis that the differential expression of the interferon pathway may have been linked to a concordant downregulation (either by silencing or mutation) of one or more of the members of the IFN signalling cascade. For example, it has been shown that in microsatellite-instability-high tumours (in particular uterine corpus endometrial cancer and stomach adenocarcinoma) a differential expression of an interferon signature is linked to the loss of function (mainly by frameshift mutations) of *JAK1* [75]. Similarly, *JAK2* mutations in non-small cell lung cancer alter the expression of the IRF1-dependent antigen presentation pathway [76]. However, I did not see any significant differential expression of the IFN signalling cascade associated with PDAC grade. I also observed interferon responsiveness of the signalling cascade as independent from the grade of cells. Nonetheless the transcriptional response to interferons was attenuated in high grade cells as compared to low grade cells. This data corroborated the hypothesis of a cell-autonomous regulatory mechanism behind the interferon gene signature, unbound from signalling events and linked to an epithelial state-specific transcriptional machinery.

VII.2 ***IRF1 mediated transcriptional regulation links the epithelial phenotype to the interferon signature***

Previous investigations, as reported in Diaferia *et al.* [3], showed the differential expression of the transcription factor IRF1 in low grade and high grade PDAC. Moreover, the analysis of grade-specific regulatory regions provided evidence of a high representation of IRF motifs in low grade-specific enhancers, as well as an extensive occupancy of these regions by IRF1 itself [3]. IRF1 is a known regulator of the late interferon response [77]. Additionally, it has also been described in a number of cancer contexts as a regulator of oncogenesis [77]. These observations allowed to hypothesise a link between the differential expression of this TF and the interferon-related signature. I confirmed that the differential expression of this TF as observed in cell lines of different grade was also a feature of patient samples. Therefore, I sought to investigate the role of IRF1 in low grade cells, using a CRISPR-Cas9-mediated loss-of-function strategy. My results showed that the ablation of this TF from these cells affects a variety of traits.

The results in this thesis provided evidence that IRF1 is in charge of controlling the main interferon-related signature in PDAC cells, and that altering its levels (either by deletion in low grade PDAC cells or by overexpression in high grade cells) results in the concordant regulation of the signature. In particular, I observed a strong regulation on the antigen processing and presentation pathway. In non-small cell lung cancer low IRF1 expression, low IFN-signature and low immunoproteasome expression are associated with a mesenchymal phenotype [78]. Similarly, in neuroblastoma, IRF1-low cell lines also display low levels of MHC I expression [79]. Interestingly, a higher expression in low MHC I cell lines could only be induced via concomitant transfection of IRF1 and NF-kB [79]. The presented results prove the role of IRF1 in PDAC as a master

regulator of the antigen processing and presentation pathway, concordant with its previously described functions [77], and that its differential expression in low *vs* high grade cells is causative of the differential activation of the antigen presentation pathway. Further functional investigations should be carried out to show that a proper and functional presentation of antigens to the immune system and sunsequent alterations of anti-tumour immunity could be achieved by altering IRF1 expression in PDACs.

VII.3 ***IRF1 regulates the antigen processing and presentation in PDAC: immune visibility and implications for immunotherapy.***

The findings of which in this work on the regulation of the antigen processing and presentation pathway in PDAC of different grade should also be discussed in terms of tumour-immune crosstalk. Understanding the immunological landscape of tumours has recently become, in fact, a remarkable field of investigation, mainly for its prognostic and predictive relevance [80].

Immunotherapy nowadays is one of the most promising fields of cancer therapy. It includes all the therapeutic approaches which use the immune system of the patient as a main tool for cancer resolution. Some examples include: immune checkpoint blockade (hacking the inhibitory co-regulation of T-cell activity by tumour cells), immunomodulatory molecules, cancer vaccines, oncolytic virus immunotherapy and adoptive chimeric T-cell therapy.

Currently available Immune checkpoints blockade therapies target PD-L1 or CTLA-4 as coregulatory molecules. Current trials in PDAC are still ongoing to provide

evidence of effectiveness [81]. I was not able to assess any difference in the expression between high grade and low grade PDAC cells of these proteins. Nonetheless I identified a substantial difference in the expression of two other co-regulatory molecules: *TNFRSF14* (or HVEM, ligand of the receptors BTLA4, CD160 and LIGHT) and *LGALS9* (or Galectin 9, ligand of TIM3). Both these molecules are highly expressed in low grade PDAC and not expressed in high PDAC, moreover, IRF1 deletion impairs their expression. TNFRSF14 and LGALS9 are involved in bidirectional co-signalling between antigen presenting cells and T-cells (but also B-cells) [82]. Moreover, the expression of both of these proteins (along with other immune suppression markers) has been shown to be predictive of PDAC patients survival [83]. It has also been shown, in a mouse model of metastatic melanoma, that a high expression of inhibitory molecules (including TNFRSF14, LGALS9 and class II MHC) is an interferon-driven mechanism of resistance to immune checkpoint blockade, and that is able to induce T-cell exhaustion [84].

My data show that cells of different grade also display a different behaviour in terms of MHC expression (both class I and class II), and that these latter are under the transcriptional control of IRF1. Also the antigen processing machinery is differentially expressed (high in low grade PDAC, low in high grade PDAC), and controlled by IRF1. As tumours themselves behave as antigen presenting cells, in the context of immune surveillance antigen processing and presentation pathway downregulation is sufficient to impair the T-cell response against the tumour [85-87].

All of the above observations should be taken into account, in the future, as potential pitfalls in the development of novel immunotherapeutic approaches against PDAC. These, in fact, would ultimately result in an inhomogeneous efficacy against cells of different grade.

Lastly, one can speculate that in PDAC the grade of histological differentiation may result in a different strategy to evade immune surveillance. In this framework, high grade cells would evade by downregulation of MHCs, while low grade cells would employ T-cell exhaustion via co-inhibitory molecules to escape immune-editing.

If so, IRF1 deficiency or sustained expression could be framed as an evolutionary adaptation process towards a challenging immune microenvironment. Whether this integrates the model of *ab initio* distinct regulatory network of tumour clones of different grade, or if this differentiation networks are a result of immune pressure has still to be investigated.

My data also provide evidence of altered microenvironmental composition upon IRF1 deletion in xenograft models, including changes in murine macrophage infiltration and collagen fibres density. The effect of IRF1 deletion, moreover, can – at least for murine macrophage infiltration– recapitulate the differential infiltration density of high and low grade PDAC cells xenografts. Immune cell and stromal recruitment has been previously associated to tumour differentiation in a number of studies. Shibuya *et al.* [88] showed a general T-cell dominated infiltration of PDACs, and provided evidence that well differentiated tumour areas are lower in $CD11b^{+}$ cells (i.e. a general macrophage marker) than poorly differentiated ones, and observed a similar trend for T-cell infiltration. Also, although CD4+ and CD8+ T-cell ratio was similar, poorly differentiated tumours showed a higher association with FoxP3+ Tregs [88]. Other work showed that macrophage infiltration (CD68+ and CD163+ cells), as well as CD25+ Tregs were associated to poorly differentiated tumours, when compared to chronic pancreatitis patients [89]. Similarly, different types of cancer-associated fibroblast have been shown to be associated to mesenchymal tumour markers (as L1CAM [89],

the latter also associated to immunosuppression [90]) [91]. These and other observations suggest a link between tumour differentiation and microenvironmental components. In the sought of better prognostic markers for PDAC, efforts have been made to analyse also the association of stromal and immune components in the general architecture of PDAC with prognosis [83, 89, 92]. Also, it has been shown that these niches could be altered by immunotherapy [93, 94], or with drugs directly targeting the stromal and extracellular compartments [91].

We may speculate that IRF1 expression could be one of the factors linking tumour cell grade to grade-specific microenvironmental niches. Analysing this peculiar role may provide a starting point for further investigations, with the aim to map the tumour cell-intrinsic factors involved in shaping PDAC microenvironment and ultimately leading to better therapeutic tools.

VII.4 ***IRF1 partly controls the epithelial state of differentiated PDAC cells***

I observed that IRF1-KO low grade cells partially lost or modified some of the epithelial phenotypes including, adhesion ability, motility, cell-to-cell contacts and growth rates. Similar, but more prominent, phenotype switches could be observed when low grade cells are deprived of epithelial specific TFs like KLF5 or ELF3 [3]. Although IRF1 has been described as a tumour suppressor able to repress the transformed phenotype [34], the observation that IRF1 occupancy in the low grade PDAC cells mainly occurs at sites with a combined IRF/AP-1 motif [3] allows to speculate that the altered epithelial phenotype may be linked to an indirect effect an low grade-specific regulatory networks. Further investigation and data mining of

already available ChIP-Seq data for epithelial-specific transcription factors in PDAC cell lines may provide a better understanding of these transcriptional dependencies. We could not rule out, however that some of these phenotypic switches may depend upon the resulting lipidic remodelling upon IRF1 deletion. It has been shown that lipidic remodelling is associated to EMT transitions [95]. The relative abundance of specific membrane lipids, in fact, has been associated to membrane fluidity and cell adhesion molecules stability [96, 97], as well as to the activation of EMT-related intracellular signalling pathways [98]. These observations allow to speculate a possible involvement of IRF1-mediated metabolic networks in changes in homotypic cell adhesion, cell motility and extracellular matrix adhesion.

VII.5 ***IRF1 is a metabolic regulator in low grade PDAC cells***

My data show that IRF1 also acts as a metabolic regulator in PDAC cells. In particular, I demonstrate that IRF1 deletion can alter the mitochondrial respiration, subvert the lipidic composition and induce lipogenesis and NADP reducing pathways.

Lipidic metabolism is one of the main metabolic targets of IRF1 regulation in low grade PDACs. I observed that IRF1 deletion results in a change in phospholipid composition, saturation and metabolism, both using RNA-Seq and metabolomics. Similarly, in adipocytes it has been shown that IRF1 expression levels affect the saturation levels of phospholipidic fatty acids [99]. The phenotype I observed may be linked to a deregulated interferon signature. It is in fact known that, mainly in response to viral infections, there is an interferon-driven alteration of cell membrane composition [100]. For example, the most strongly downregulated transcript in IRF1-KO low grade cells, *RARRES3*, is a well-known IRF1 target [101] and has a strong phospholipase activity [102]. One may therefore speculate that the observations of

altered ECM adhesion, homotypic adhesion and microenvironmental changes upon IRF1 deletion, may be linked to changes in cell membrane composition (see above) [103].

As per Daemen *et al.* [20], it has been shown that the "*epithelial*" (low grade) phenotype is linked to a lipogenic profile, while a "*quasi-mesenchymal*" phenotype is associated to a glycolytic profile [20]. Nonetheless, IRF1 deletion in low grade cells is causing a further increase in lipogenesis, as shown in the presented carbon flux tracing experiment. In addition, no change in glycolysis could be observed, while increases in in parallel pathways like the pentose phosphate pathway and the anaplerosis of the TCA cycle via the activity of malic enzymes could be appreciated. This suggests that IRF1 may act as a suppressor of lipogenesis in low grade cells, as its deletion further unleashes the already active synthesis of lipids. Our final model also links the pentose phosphate pathway and malic enzyme activity to increased lipogenesis, as both involve NADP reduction to NADPH. Importantly, NADPH serves as an electron donor during lipid synthesis. As said before, however, high grade cell lines have been shown to have a poorly lipogenic metabolism [20]. IRF1 deletion in low grade cells, in contrast, was not able to repress lipogenesis, thus ruling out the possibility that this TF has a differential role in controlling the metabolism of the two groups. Nonetheless, a more profound investigation of its control on metabolism may be needed, possibly by analysing the metabolic effects of IRF1 ectopic expression in high grade cells.

From respirometric analysis, I observed a substantial increase in the activity of complexes of the respiratory chain, as well as a general upregulation in the activity of the pathway, whether or not it was coupled to ATP synthesis. In fact, metabolomics data show no significant increase in the intracellular ATP pool.

One can speculate that in low grade PDAC cells, IRF1 acts as a repressor of oxidative stress, and its deletion leads to an increase in mitochondrial activation and as such may serve to increase reactive oxygen species production. Moreover, transcriptional upregulation of genes encoding for ROS-detoxifying proteins as Thioredoxin Reductase 1 (*TXNRD1*) and Quiescin Sulfhydryl Oxidase 1 (*QSOX1*) was observed. The latter, coupled with an increase in NADPH production could indicate a role for IRF1 in ROS detoxification. Further investigations about the oxidative stress to which IRF1-KO low grade PDAC cells may undergo should however be needed.

The relevance of IRF1 expression in the regulation of an interferon signature also allows to speculate that IRF1 expression may mediate metabolic cross-communication with the immune system. These pathways of immune-tumour crosstalk have, in fact, become an interesting open field of research [104]. For example, it has been shown in melanoma that IRF1 low expression is linked to a high glycolytic activity, and that this latter is the mediator of a reduced anti-tumoural T-cell activity [105]. It may be of great interest to address whether PDAC cell grade and grade specific metabolic pathways could be studied as mediators of differential immune response.

VII.6 ***Interferon signature, PDAC grade and chemotherapy***

In search of alternative therapies for pancreatic cancer, the presented findings could pave the way for more comprehensive and efficacious treatments. Understanding heterogeneous behaviours, in fact, would result in a more precise targeting of all the different components of PDAC.

A number of interferon-related signatures have previously proved to be prognostic markers of therapy efficacy. Most of the current knowledgebase links this signature to a lower response of different solid tumours to DNA-damaging agents. This has been

shown for squamous cell carcinoma resistance to radiotherapy and for breast cancer where a meta-analysis of survival data validated a similar resistance to radiation therapy [48]. Similarly, breast cancer resistance to anthracyclins and melanoma resistance to MEK inhibitors have been associated with an IFN signature [49, 50]. State-of-the-art therapies for pancreatic cancer, nonetheless, are mostly based on DNA-damaging agents, such as gemcitabine (usually in a combination with paclitaxel) or the standardised FOLFIRINOX formulation (Folic acid; 5-Fluorouracil, Irinotecan and Oxaliplatin) [4]. Moreover, it has been shown by Collisson *et al.* that the "*quasi-mesenchymal*" (i.e. high grade cells) subtype of PDAC cells are more sensitive to gemcitabine treatment as compared to the "*epithelial*" ones [5].These observations may lead to speculate that the poor responses to therapy of PDAC patients could be linked to a selective therapy which could only ablate a non-resistant subpopulation, *i.e.* high grade tumour cells, and that the active interferon signature of low grade cells may be the mediator of such resistance.

VIII. Acknowledgments

The biochemical investigations of sections V.8 and V.9 were performed, analysed and interpreted by Matteo Audano, Silvia Pedretti and Nico Mitro, in Mitro lab at Dipartimento di Scienze Farmacologiche e Biomolecolari, University of Milan.

RNA-seq data were analysed by Chiara Balestrieri at Gioacchino Natoli lab, Humanitas University, Rozzano (MI).

IX. References

1. Dunne, R.F. and A.F. Hezel, *Genetics and Biology of Pancreatic Ductal Adenocarcinoma*. Hematology/oncology clinics of North America, 2015. **29**(4): p. 595-608.
2. Kloppel, G., et al., *Histological and fine structural features of pancreatic ductal adenocarcinomas in relation to growth and prognosis: studies in xenografted tumours and clinico-histopathological correlation in a series of 75 cases*. Histopathology, 1985. **9**(8): p. 841-56.
3. Diaferia, G.R., et al., *Dissection of transcriptional and cis-regulatory control of differentiation in human pancreatic cancer*. EMBO J, 2016. **35**(6): p. 595-617.
4. Chiaravalli, M., M. Reni, and E.M. O'Reilly, *Pancreatic ductal adenocarcinoma: State-of-the-art 2017 and new therapeutic strategies*. Cancer treatment reviews, 2017. **60**: p. 32-43.
5. Collisson, E.A., et al., *Subtypes of pancreatic ductal adenocarcinoma and their differing responses to therapy*. Nat Med, 2011. **17**(4): p. 500-3.
6. Bailey, P., et al., *Genomic analyses identify molecular subtypes of pancreatic cancer*. Nature, 2016. **531**(7592): p. 47-52.
7. Ilic, M. and I. Ilic, *Epidemiology of pancreatic cancer*. World Journal of Gastroenterology, 2016. **22**(44): p. 9694-9705.
8. Chandrakanth, A., et al., *Predictive global trends in the incidence and mortality of pancreatic cancer based on geographic location, socio-economic status, and demographic shift*. Journal of Surgical Oncology, 2016. **114**(6): p. 736-742.
9. Rahib, L., et al., *Projecting Cancer Incidence and Deaths to 2030: The Unexpected Burden of Thyroid, Liver, and Pancreas Cancers in the United States*. Cancer Research, 2014. **74**(11): p. 2913-2921.
10. Makohon-Moore, A. and C.A. Iacobuzio-Donahue, *Pancreatic cancer biology and genetics from an evolutionary perspective*. Nature reviews. Cancer, 2016. **16**(9): p. 553-565.
11. Waddell, N., et al., *Whole genomes redefine the mutational landscape of pancreatic cancer*. Nature, 2015. **518**(7540): p. 495-501.
12. Makohon-Moore, A.P., et al., *Precancerous neoplastic cells can move through the pancreatic ductal system*. Nature, 2018. **561**(7722): p. 201-205.
13. Notta, F., et al., *A renewed model of pancreatic cancer evolution based on genomic rearrangement patterns*. Nature, 2016. **538**(7625): p. 378-382.
14. Kleeff, J., et al., *Pancreatic cancer*. Nat Rev Dis Primers, 2016. **2**: p. 16022.
15. Hezel, A.F., et al., *Genetics and biology of pancreatic ductal adenocarcinoma*. Genes & Development, 2006. **20**(10): p. 1218-1249.
16. Network, C.G.A.R., *Integrated Genomic Characterization of Pancreatic Ductal Adenocarcinoma*. Cancer Cell, 2017. **32**(2): p. 185-203 e13.
17. Moffitt, R.A., et al., *Virtual microdissection identifies distinct tumor- and stroma-specific subtypes of pancreatic ductal adenocarcinoma*. Nature genetics, 2015. **47**(10): p. 1168-1178.
18. Witkiewicz, A.K., et al., *Whole-exome sequencing of pancreatic cancer defines genetic diversity and therapeutic targets*. Nat Commun, 2015. **6**: p. 6744.

19. Lomberk, G., et al., *Distinct epigenetic landscapes underlie the pathobiology of pancreatic cancer subtypes*. Nat Commun, 2018. **9**.
20. Daemen, A., et al., *Metabolite profiling stratifies pancreatic ductal adenocarcinomas into subtypes with distinct sensitivities to metabolic inhibitors*. Proceedings of the National Academy of Sciences of the United States of America, 2015. **112**(32): p. 7.
21. Balestrieri, C., et al., *Co-optation of Tandem DNA Repeats for the Maintenance of Mesenchymal Identity*. Cell, 2018. **173**(5): p. 1150-1164 e14.
22. Parker, B.S., J. Rautela, and P.J. Hertzog, *Antitumour actions of interferons: implications for cancer therapy*. Nat Rev Cancer, 2016. **16**(3): p. 131-44.
23. Chen, H.M., et al., *Critical role for constitutive type I interferon signaling in the prevention of cellular transformation*. Cancer Sci, 2009. **100**(3): p. 449-56.
24. Donnelly, R.P. and S.V. Kotenko, *Interferon-lambda: a new addition to an old family*. J Interferon Cytokine Res, 2010. **30**(8): p. 555-64.
25. Platanias, L.C., *Mechanisms of type-I- and type-II-interferon-mediated signalling*. Nat Rev Immunol, 2005. **5**(5): p. 375-86.
26. Zhou, F., *Molecular mechanisms of IFN-gamma to up-regulate MHC class I antigen processing and presentation*. Int Rev Immunol, 2009. **28**(3-4): p. 239-60.
27. Miyamoto, M., et al., *Regulated expression of a gene encoding a nuclear factor, IRF-1, that specifically binds to IFN-β gene regulatory elements*. Cell, 1988. **54**(6): p. 903-913.
28. Savitsky, D., et al., *Regulation of immunity and oncogenesis by the IRF transcription factor family*. Cancer Immunol Immunother, 2010. **59**(4): p. 489-510.
29. Glasmacher, E., S. Agrawal, and A.B. Chang, *A genomic regulatory element that directs assembly and function of immune-specific AP-1-IRF complexes*. Science, 2012(November).
30. Li, P., et al., *BATF-JUN is critical for IRF4-mediated transcription in T cells*. Nature, 2012. **490**(7421): p. 543-6.
31. Mancino, A., et al., *A dual cis-regulatory code links IRF8 to constitutive and inducible gene expression in macrophages*. Genes Dev, 2015. **29**(4): p. 394-408.
32. Takaoka, A., T. Tamura, and T. Taniguchi, *Interferon regulatory factor family of transcription factors and regulation of oncogenesis*. Cancer Sci, 2008. **99**(3): p. 467-78.
33. Harada, H., et al., *Anti-oncogenic and oncogenic potentials of interferon regulatory factors-1 and -2*. Science, 1993. **259**(5097): p. 971-4.
34. Tanaka, N., et al., *Cellular commitment to oncogene-induced transformation or apoptosis is dependent on the transcription factor IRF-1*. Cell, 1994. **77**(6): p. 829-39.
35. Tanaka, N., et al., *Cooperation of the tumour suppressors IRF-1 and p53 in response to DNA damage*. Nature, 1996. **382**: p. 816.
36. Yang, J., et al., *Epigenetic silencing of IRF1 dysregulates type III interferon responses to respiratory virus infection in epithelial to mesenchymal transition*. Nat Microbiol, 2017. **2**(June): p. 17086.
37. Tamura, G., et al., *Two Distinct Regions of Deletion on the Long Arm of Chromosome 5 in Differentiated Adenocarcinomas of the Stomach*. Cancer Research, 1996. **56**(3): p. 612-615.

38. Nozawa, H., et al., *Functionally inactivating point mutation in the tumor-suppressor IRF-1 gene identified in human gastric cancer*. International Journal of Cancer, 1998. **77**(4): p. 522-527.
39. Peralta, R.C., et al., *Distinct regions of frequent loss of heterozygosity of chromosome 5p and 5q in human esophageal cancer*. International Journal of Cancer, 1998. **78**(5): p. 600-605.
40. Cavalli, L.R., et al., *Frequent loss of heterozygosity at the interferon regulatory factor-1 gene locus in breast cancer*. Breast Cancer Res Treat, 2010. **121**(1): p. 227-31.
41. Bouker, K.B., et al., *Interferon regulatory factor-1 (IRF-1) exhibits tumor suppressor activities in breast cancer associated with caspase activation and induction of apoptosis*. Carcinogenesis, 2005. **26**(9): p. 1527-35.
42. Sakai, T., et al., *The roles of interferon regulatory factors 1 and 2 in the progression of human pancreatic cancer*. Pancreas, 2014. **43**(6): p. 909-16.
43. Monsurrò, V., et al., *Anti-viral state segregates two molecular phenotypes of pancreatic adenocarcinoma: potential relevance for adenoviral gene therapy*. Journal of Translational Medicine, 2010. **8**(1): p. 10.
44. Hoshikawa, M., et al., *NK cell and IFN signatures are positive prognostic biomarkers for resectable pancreatic cancer*. Biochem Biophys Res Commun, 2018. **495**(2): p. 2058-2065.
45. Doherty, M.R., et al., *Interferon-beta represses cancer stem cell properties in triple-negative breast cancer*. Proc Natl Acad Sci U S A, 2017. **114**(52): p. 13792-13797.
46. Michaut, M., et al., *Integration of genomic, transcriptomic and proteomic data identifies two biologically distinct subtypes of invasive lobular breast cancer*. Scientific Reports, 2016. **6**: p. 18517.
47. Tong, R., et al., *Decreased Interferon Alpha/Beta Signature Associated with Human Lung Tumorigenesis*. J Interferon Cytokine Res, 2015. **35**(12): p. 963-8.
48. Weichselbaum, R.R., et al., *An interferon-related gene signature for DNA damage resistance is a predictive marker for chemotherapy and radiation for breast cancer*. Proceedings of the National Academy of Sciences of the United States of America, 2008. **105**(47): p. 18490-18495.
49. Sistigu, A., et al., *Cancer cell-autonomous contribution of type I interferon signaling to the efficacy of chemotherapy*. Nat Med, 2014. **20**(11): p. 1301-9.
50. Litvin, O., et al., *Interferon alpha/beta Enhances the Cytotoxic Response of MEK Inhibition in Melanoma*. Mol Cell, 2015. **57**(5): p. 784-96.
51. Bryant, K.L., et al., *KRAS: feeding pancreatic cancer proliferation*. Trends Biochem Sci, 2014. **39**(2): p. 91-100.
52. Ying, H., et al., *Oncogenic Kras maintains pancreatic tumors through regulation of anabolic glucose metabolism*. Cell, 2012. **149**(3): p. 656-70.
53. Son, J., et al., *Glutamine supports pancreatic cancer growth through a KRAS-regulated metabolic pathway*. Nature, 2013. **496**(7443): p. 101-5.
54. Dey, P., et al., *Genomic deletion of malic enzyme 2 confers collateral lethality in pancreatic cancer*. Nature, 2017. **542**(7639): p. 119-123.
55. Zhang, G., et al., *Integration of Metabolomics and Transcriptomics Revealed a Fatty Acid Network Exerting Growth Inhibitory Effects in Human Pancreatic Cancer*. Clinical cancer research : an official journal of the American Association for Cancer Research, 2013. **19**(18): p. 4983-4993.

56. Guillaumond, F., et al., *Cholesterol uptake disruption, in association with chemotherapy, is a promising combined metabolic therapy for pancreatic adenocarcinoma*. Proc Natl Acad Sci U S A, 2015. **112**(8): p. 2473-8.
57. McDonald, O.G., et al., *Epigenomic reprogramming during pancreatic cancer progression links anabolic glucose metabolism to distant metastasis*. Nat Genet, 2017. **49**(3): p. 367-376.
58. Vasseur, S., et al., *Hypoxia induced tumor metabolic switch contributes to pancreatic cancer aggressiveness*. Cancers (Basel), 2010. **2**(4): p. 2138-52.
59. Guillaumond, F., et al., *Strengthened glycolysis under hypoxia supports tumor symbiosis and hexosamine biosynthesis in pancreatic adenocarcinoma*. Proc Natl Acad Sci U S A, 2013. **110**(10): p. 3919-24.
60. Chen, Z.H., H. Zhang, and T.M. Savarese, *Gene deletion chemoselectivity: codeletion of the genes for p16(INK4), methylthioadenosine phosphorylase, and the alpha- and beta-interferons in human pancreatic cell carcinoma lines and its implications for chemotherapy*. Cancer research, 1996. **56**(5): p. 1083-1090.
61. Huang da, W., B.T. Sherman, and R.A. Lempicki, *Systematic and integrative analysis of large gene lists using DAVID bioinformatics resources*. Nat Protoc, 2009. **4**(1): p. 44-57.
62. Subramanian, A., et al., *Gene set enrichment analysis: a knowledge-based approach for interpreting genome-wide expression profiles*. Proc Natl Acad Sci U S A, 2005. **102**(43): p. 15545-50.
63. Xia, J. and D.S. Wishart, *Using MetaboAnalyst 3.0 for Comprehensive Metabolomics Data Analysis*. Current Protocols in Bioinformatics, 2016. **55**(1): p. 14.10.1-14.10.91.
64. Bankhead, P., et al., *QuPath: Open source software for digital pathology image analysis*. Scientific Reports, 2017. **7**(1): p. 16878.
65. Sanjana, N.E., O. Shalem, and F. Zhang, *Improved vectors and genome-wide libraries for CRISPR screening*. Nat Methods, 2014. **11**(8): p. 783-784.
66. Ran, F.A., et al., *Genome engineering using the CRISPR-Cas9 system*. Nat Protoc, 2013. **8**(11): p. 2281-2308.
67. Picelli, S., et al., *Smart-seq2 for sensitive full-length transcriptome profiling in single cells*. Nat Methods, 2013. **10**(11): p. 1096-8.
68. Picelli, S., et al., *Tn5 transposase and tagmentation procedures for massively scaled sequencing projects*. Genome research, 2014. **24**(12): p. 2033-40.
69. Trapnell, C., et al., *Differential gene and transcript expression analysis of RNA-seq experiments with TopHat and Cufflinks*. Nat Protoc, 2012. **7**(3): p. 562-78.
70. Liao, Y., G.K. Smyth, and W. Shi, *featureCounts: an efficient general purpose program for assigning sequence reads to genomic features*. Bioinformatics (Oxford, England), 2014. **30**(7): p. 923-30.
71. Robinson, M.D., D.J. McCarthy, and G.K. Smyth, *edgeR: a Bioconductor package for differential expression analysis of digital gene expression data*. Bioinformatics, 2010. **26**(1): p. 139-40.
72. Supek, F., et al., *REVIGO Summarizes and Visualizes Long Lists of Gene Ontology Terms*. PLOS ONE, 2011. **6**(7): p. e21800.
73. Audano, M., et al., *Zc3h10 is a novel mitochondrial regulator*. EMBO reports, 2018. **19**(4).
74. Sinha, A., et al., *Mesenchymal-like pancreatic cancer cells harbor specific genomic alterations more frequently than their epithelial-like counterparts*. Molecular oncology, 2014. **8**(7): p. 1253-65.

75. Albacker, L.A., et al., *Loss of function JAK1 mutations occur at high frequency in cancers with microsatellite instability and are suggestive of immune evasion*. PLoS ONE, 2017. **12**(11): p. e0176181.
76. Shen, T., et al., *Genetic defects of the IRF1-mediated major histocompatibility complex class I antigen presentation pathway occur prevalently in the JAK2 gene in non-small cell lung cancer*. Oncotarget, 2017. **8**(37): p. 60975-60986.
77. Zhao, G.-N., D.-S. Jiang, and H. Li, *Interferon regulatory factors: at the crossroads of immunity, metabolism, and disease*. Biochimica et Biophysica Acta (BBA) - Molecular Basis of Disease, 2015. **1852**(2): p. 365-378.
78. Tripathi, S.C., H.L. Peters, and A. Taguchi, *Immunoproteasome deficiency is a feature of non-small cell lung cancer with a mesenchymal phenotype and is associated with a poor outcome*. Proceedings of the ..., 2016.
79. Lorenzi, S., et al., *IRF1 and NF-kB Restore MHC Class I-Restricted Tumor Antigen Processing and Presentation to Cytotoxic T Cells in Aggressive Neuroblastoma*. PLOS ONE, 2012. **7**(10): p. e46928.
80. Thorsson, V., et al., *The Immune Landscape of Cancer*. Immunity, 2018. **48**(4): p. 812-830.e14.
81. Thind, K., et al., *Immunotherapy in pancreatic cancer treatment: a new frontier*. Therapeutic advances in gastroenterology, 2017. **10**(1): p. 168-194.
82. Chen, L. and D.B. Flies, *Molecular mechanisms of T cell co-stimulation and co-inhibition*. Nat Rev Immunol, 2013. **13**(4): p. 227-42.
83. Sideras, K., et al., *Tumor cell expression of immune inhibitory molecules and tumor-infiltrating lymphocyte count predict cancer-specific survival in pancreatic and ampullary cancer*. Int J Cancer, 2017. **141**(3): p. 572-582.
84. Benci, J.L., et al., *Tumor Interferon Signaling Regulates a Multigenic Resistance Program to Immune Checkpoint Blockade*. Cell, 2016. **167**(6): p. 1540-1554 e12.
85. DuPage, M., et al., *Expression of tumour-specific antigens underlies cancer immunoediting*. Nature, 2012. **482**: p. 405.
86. Matsushita, H., et al., *Cancer exome analysis reveals a T-cell-dependent mechanism of cancer immunoediting*. Nature, 2012. **482**: p. 400.
87. Thibodeau, J., M.C. Bourgeois-Daigneault, and R. Lapointe, *Targeting the MHC Class II antigen presentation pathway in cancer immunotherapy*. Oncoimmunology, 2012. **1**(6): p. 908-916.
88. Shibuya, K.C., et al., *Pancreatic ductal adenocarcinoma contains an effector and regulatory immune cell infiltrate that is altered by multimodal neoadjuvant treatment*. PLoS One, 2014. **9**(5): p. e96565.
89. Helm, O., et al., *Comparative characterization of stroma cells and ductal epithelium in chronic pancreatitis and pancreatic ductal adenocarcinoma*. PloS one, 2014. **9**(5): p. e94357-e94357.
90. Grage-Griebenow, E., et al., *L1CAM promotes enrichment of immunosuppressive T cells in human pancreatic cancer correlating with malignant progression*. Molecular oncology, 2014. **8**(5): p. 982-997.
91. Nielsen, M.F.B., M.B. Mortensen, and S. Detlefsen, *Key players in pancreatic cancer-stroma interaction: Cancer-associated fibroblasts, endothelial and inflammatory cells*. World journal of gastroenterology, 2016. **22**(9): p. 2678-2700.
92. Carstens, J.L., et al., *Spatial computation of intratumoral T cells correlates with survival of patients with pancreatic cancer*. Nature Communications, 2017. **8**: p. 15095.

93. Tsujikawa, T., et al., *Quantitative Multiplex Immunohistochemistry Reveals Myeloid-Inflamed Tumor-Immune Complexity Associated with Poor Prognosis*. Cell Rep, 2017. **19**(1): p. 203-217.
94. Zhu, Y., et al., *CSF1/CSF1R blockade reprograms tumor-infiltrating macrophages and improves response to T-cell checkpoint immunotherapy in pancreatic cancer models*. Cancer Res, 2014. **74**(18): p. 5057-69.
95. Morandi, A., et al., *Targeting the Metabolic Reprogramming That Controls Epithelial-to-Mesenchymal Transition in Aggressive Tumors*. Frontiers in Oncology, 2017. **7**(40).
96. Mathow, D., et al., *Zeb 1 affects epithelial cell adhesion by diverting glycosphingolipid metabolism*. 2015. **16**(3): p. 321-331.
97. Márquez, M.G., et al., *Changes in membrane lipid composition cause alterations in epithelial cell-cell adhesion structures in renal papillary collecting duct cells*. Biochimica et Biophysica Acta (BBA) - Biomembranes, 2012. **1818**(3): p. 491-501.
98. Sánchez-Martínez, R., et al., *A link between lipid metabolism and epithelial-mesenchymal transition provides a target for colon cancer therapy*. Oncotarget, 2015. **6**(36): p. 38719-38736.
99. Friesen, M., et al., *Activation of IRF1 in Human Adipocytes Leads to Phenotypes Associated with Metabolic Disease*. Stem Cell Reports, 2017. **8**(5): p. 1164-1173.
100. Schoggins, John W. and G. Randall, *Lipids in Innate Antiviral Defense*. Cell Host & Microbe, 2013. **14**(4): p. 379-385.
101. Sers, C., et al., *The class II tumour suppressor gene H-REV107-1 is a target of interferon-regulatory factor-1 and is involved in IFN g -induced cell death in human ovarian carcinoma cells*. 2002(January): p. 2829-2839.
102. Mardian, E.B., R.M. Bradley, and R.E. Duncan, *The HRASLS (PLA/AT) subfamily of enzymes*. J Biomed Sci, 2015. **22**: p. 99.
103. Beloribi-Djefaflia, S., S. Vasseur, and F. Guillaumond, *Lipid metabolic reprogramming in cancer cells*. Oncogenesis, 2016. **5**: p. e189.
104. Renner, K., et al., *Metabolic Hallmarks of Tumor and Immune Cells in the Tumor Microenvironment*. Frontiers in Immunology, 2017. **8**(248).
105. Cascone, T., et al., *Increased Tumor Glycolysis Characterizes Immune Resistance to Adoptive T Cell Therapy*. Cell Metabolism, 2018. **27**(5): p. 977-987.e4.